NASA TECHNICAL NOTE

NASA TN D-5456

NASA TN D-5456

ANALYSIS AND EVALUATION OF A NOVEL INERTIAL NAVIGATION SYSTEM

by Edmund J. Koenke

Electronics Research Center

Cambridge, Mass.

NATIONAL AERONAUTICS AND SPACE ADMINISTRATION • WASHINGTON, D. C. • NOVEMBER 1969

1. Report No.	2. Government Accession No.	3. Recipient's Catalog No.
NASA TN D-5456		

4. Title and Subtitle	5. Report Date
Analysis and Evaluation of a Novel Inertial Navigation System	November 1969
	6. Performing Organization Code
7. Author(s)	8. Performing Organization Report No. C-79
9. Performing Organization Name and Address Electronics Research Center Cambridge, Mass. 02139	10. Work Unit No. 180-17-05-07
	11. Contract or Grant No.
	13. Type of Report and Period Covered
12. Sponsoring Agency Name and Address National Aeronautics and Space Administration Washington, D.C. 20546	Technical Note
	14. Sponsoring Agency Code

15. Supplementary Notes

16. Abstract

A novel inertial navigation system referred to in the literature as the RAMP inertial navigator is analyzed and then compared to a conventional local vertical navigation system. The main attraction of this system is that it is capable of indicating the vertical using only gyros as sensors. The theory of the system mechanization is developed from first principles and methods for calculation of the system loop gains are presented. First, a single-axis system is considered and then the analysis is generalized to a three-axis system. The analyses performed indicate that error propagation for the novel system and the conventional system are identical for identical error sources. It is also shown that the RAMP base motion isolation system provides a better gyro environment than that used in a conventional system since the level gyros are not required in the gimbal servo loops. Reports of flight tests of this system corroborate these conclusions.

17. Key Words
INERTIAL
NAVIGATION
Gyroscopes
Sensors
Error Propagation

18. Distribution Statement
Unclassified - Unlimited

19. Security Classif. (of this report)	20. Security Classif. (of this page)	21. No. of Pages	22. Price
Unclassified	Unclassified	56	$3.00 *

*For sale by the Clearinghouse for Federal Scientific and Technical Information
Springfield, Virginia 22151

ANALYSIS AND EVALUATION

of a

NOVEL INERTIAL NAVIGATION SYSTEM*

By Edmund J. Koenke

Electronics Research Center

SUMMARY

A novel inertial navigation system referred to in the literature as the RAMP inertial navigator is analyzed and then compared to a conventional local vertical navigation system. The main attraction of this system is that it is capable of indicating the vertical using only gyros as sensors. The theory of the system mechanization is developed from first principles and methods for calculation of the system loop gains are presented. First, a single-axis system is considered and then the analysis is generalized to a three-axis system. The analyses performed indicate that error propagation for the novel system and the conventional system are identical for identical error sources. It is also shown that the RAMP base motion isolation system provides a better gyro environment than that used in a conventional system since the level gyros are not required in the gimbal servo loops. Reports of flight tests of this system corroborate these conclusions.

---

*Submitted to the Department of Aeronautics and Astronautics, Massachusetts Institute of Technology, on May 24, 1969, in partial fulfillment of the requirements for the degree of Master of Science.

I. INTRODUCTION

In 1959 K. J. Astrom and N. F. Hector (ref. 1) published a report discussing a technique for indication of the vertical with a pendulum by electromechanically synthesizing a large moment of inertia. Since then (refs. 2,3), additional papers have been published with a report on methods of using the principle discussed in reference 1 to mechanize a local vertical navigator. This system was built by the Swedish Phillips Co. Ltd. and flight tested. Results of the flight tests appear in reference 3 which was published in 1968.

The system called the RAMP (Rate and Acceleration Measuring Pendulum) system is also discussed briefly in reference 4. It consists of three gyros only (i.e., no accelerometers).Reference 3 reports a high degree of navigation accuracy using fire control quality gyros. As a result of these data, this work has as its prime objective to explain how high navigational accuracy can be obtained with low quality sensors. To this end, a complete analysis of the system is performed. First, a method of vertical indication, discussed in reference 1, is presented. A single-axis mechanization of the system is then analyzed and compared with a conventional (gyro and accelerometer) single-axis local vertical navigator. As a prelude to a three-axis mechanization and analysis, a base motion isolation system is also presented. Comparison of a three-axis mechanization with a conventional three-axis local vertical navigator is then made.

The numerical calculations and approximations used in this analysis are identical to those used in reference 5 and are presented below:

Vehicle Motion Data

$$r\ddot{L}_{max} = r\ddot{\lambda}_{max} = 0.5g$$

$$\dot{r}_{max} = 100 \text{ ft/sec}$$

$$\dot{L}_{max} = \dot{\lambda}_{max} = 1.6 \times 10^{-4} \text{ rad/sec}$$

$$\ddot{r}_{max} = 2g$$

System Design Data

$$\delta L_{max} = \delta\lambda_{max} = 10 \text{ min} = 2.9 \times 10^{-3} \text{ rad}$$

$$\delta\dot{L}_{max} = \delta\dot{\lambda}_{max} = \delta L_{max}\omega_s = 3.6 \times 10^{-6} \text{ rad/sec}$$

$$\delta\ddot{L}_{max} = \delta\ddot{\lambda}_{max} = \delta L_{max}\omega_s^2 = 4.5 \times 10^{-9} \text{ rad/sec}$$

$$\delta\dddot{L}_{max} = \delta\dddot{\lambda}_{max} = \delta L_{max}\omega_s^3 = 5.6 \times 10^{-12} \text{ rad/sec}$$

$$\delta h_{max} = 2000 \text{ ft}$$

$$\delta\dot{h}_{max} = \delta h_{max}\omega_s = 2.5 \text{ ft/sec}$$

In addition, all terms with magnitudes less than 2×10^{-5} g were considered negligible for the purposes of the analyses conducted in this work.

The primary conclusion resulting from these analyses is that the error-propagation mechanism for both the RAMP navigator and for a conventional navigator are identical for identical error sources. The question of high-accuracy navigation with fire control quality gyros is answered by the hypothesis that the gyros, although of low quality, are stable over the flight time, but may exhibit large shifts from warm-up to warm-up, thus necessitating recalibration before each flight. An alternative hypothesis contends that if the gyros are sensitive to float motions, then better performance will be achieved in the RAMP system because of its superior base motion isolation system.

NOMENCLATURE

A_g	Gyro float angle
C_g	Gyro damping coefficient
C_i^j	Transformation matrix from frame i to frame j
C_v	Correction to the vertical
D	Deviation of the normal
e	Ellipticity of Earth
$\bar{F}$	Sum of forces on pendulum bob
F(p)	Pendulum feedback gain

$\bar{f}^p$	Specific force in the instrumented frame
$\bar{G}$	Gravitational field vector
$\bar{g}$	Local gravity vector
H_s	Gyro spin angular momentum
$\bar{H}$	Angular momentum vector
h	Altitude
[I]	Inertia matrix
I_{CM}	Inertia of controlled member about rotational axis
I_g	Gyro moment of inertia
I_p	Moment of inertia of pendulum about its rotational axis
K_1	Gain
K'_g	Gyro spring constant
K_T, K_g	Gyro loop gains
k^2	Radius of gyration
L	Latitude (geographic)
L_c	Latitude (computed)
L_g	Latitude (geocentric)
ℓ	Longitude (Earth referenced)
$\bar{M}_{APP}$	Externally applied torque
M_{CM}	Command torque to controlled member
$\bar{M}_m$	Torque motor commands
$\bar{M}_p$	Sum of torques on pendulum pivot
m	Mass of pendulum
R	Magnitude of $\bar{r}$
$\bar{r}$	Position vector

r_L	Radius of curvature in meridian plane
r_ℓ	Radius of curvature in comeridian plane
T_1, T_2	Time constants
T_g	Gyro time constant
$(u)f$	Accelerometer uncertainty
$(u)M_{CM}$	Uncertainty in M_{CM}
$(u)M_p$	Uncertainty in M_p
$(u)W_g$	Gyro uncertainties in angular velocity
W_{CM}	Natural frequency of controlled member servo loop
W_{CMD}	Gyro command angular velocity
W_{IA}	Angular velocity about gyro input axis
$\overline{W}_{ip}$	Angular velocity of pendulum w.r. to inertial reference
W_{OA}	Angular velocity about the gyro output axis
W_S	Schuler frequency
W_{SRA}	Angular velocity about the gyro spin reference axis
$\overline{\alpha}_p$	Acceleration of pendulum pivot
ξ, η	Deflection of the vertical
δh	Error in altitude
δL	Latitude error
$\delta \ell$	Longitude error (Earth referenced)
$\delta \lambda$	Longitude error (celestial)
$\delta \theta$	Single axis position error
$\delta \theta$	Single axis velocity error
θ_{CMp}	Angle between controlled member and pendulum
θ_{iCM}	Angle between controlled member and inertial reference

θ_{ivC}	Computed angle between vertical and inertial reference
θ_{iv}	Angle between vertical and inertial reference
θ_{ip}	Angle between pendulum and inertial reference
θ_{vp}	Angle between pendulum and vertical
λ	Longitude (celestial)
ρ	Distance from pendulum pivot to pendulum bob
σ_M^2	Variance of $(u)M_p$
σ_W^2	Variance of $(u)W_g$
Φ, θ, ψ	Gimbal angles
ω_{ie}	Earth angular velocity

Subscripts and superscripts

b	body frame	n	navigational frame
c	inertial frame	max	maximum
i	inertial frame	CM	controlled member
e	Earth frame	v	vertical

Operators

δ	variational operator	p	heaviside operator
		s	Laplace operator

II. INDICATION OF THE VERTICAL WITH A PENDULUM

Indication of the vertical is essentially the only requirement for navigating over the surface of the Earth, since both latitude and longitude are implicit in the determination of the direction of the local vertical with respect to an Earth-centered inertial coordinate frame. This is illustrated in Figure 1.

Note that precise altitude information is not contained in the knowledge of the vertical and must be separately determined if it is necessary. Methods of vertical indication with a pendulum are discussed in references 1, 4, 5, 6, 7, 8 and 9 and will be repeated in this study since this is the basic principle underlying the mechanization of the RAMP navigator.

Begin with a consideration of a simple pendulum, constrained to move in one plane, and with the pivot of the pendulum accelerated

over the surface of a spherical, non rotating Earth. Such a device is illustrated in Figure 2.

From basic geometry, it is seen that

$$\theta_{iv} + \theta_{vp} = \theta_{ip} \tag{1}$$

The rotational motion of the pendulum bob about the pendulum pivot is described by the equation for rigid-body rotational motion from basic mechanics, namely:

$$p_i \bar{H}_p = \bar{M}_p. \tag{2}$$

From Figure 2 it is readily observed that

$$\bar{M}_p = \bar{\rho} \times \bar{F} \tag{3}$$

and that

$$\bar{F} = m(\bar{G} - \bar{\alpha}_p). \tag{4}$$

Also, it is easily verified that if a small angle θ_{vp} is assumed, then the vectors $\bar{G}^i$, $\bar{\alpha}_p^i$, $\bar{\rho}^i$ are approximated by

$$\bar{G}^i = \begin{Bmatrix} -G \cos \theta_{iv} \\ 0 \\ -G \sin \theta_{iv} \end{Bmatrix} \tag{5}$$

$$\bar{\alpha}_p^i = \begin{Bmatrix} -R\ddot{\theta}_{iv} \sin \theta_{iv} \\ 0 \\ R\ddot{\theta}_{iv} \cos \theta_{iv} \end{Bmatrix} \tag{6}$$

$$\bar{\rho}^i = \begin{Bmatrix} -\rho \cos \theta_{ip} \\ 0 \\ -\rho \sin \theta_{ip} \end{Bmatrix} \tag{7}$$

Again, recall from the mechanics of a rigid body that

$$\bar{H}_p^i = [I]\, \bar{W}_{ip}^i \tag{8}$$

where

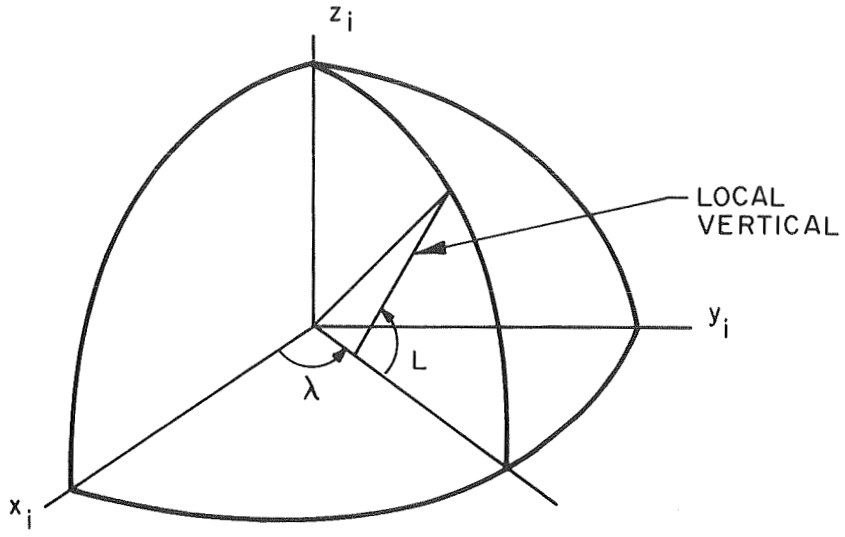

Figure 1.- Geometric relation of the vertical to latitude and longitude

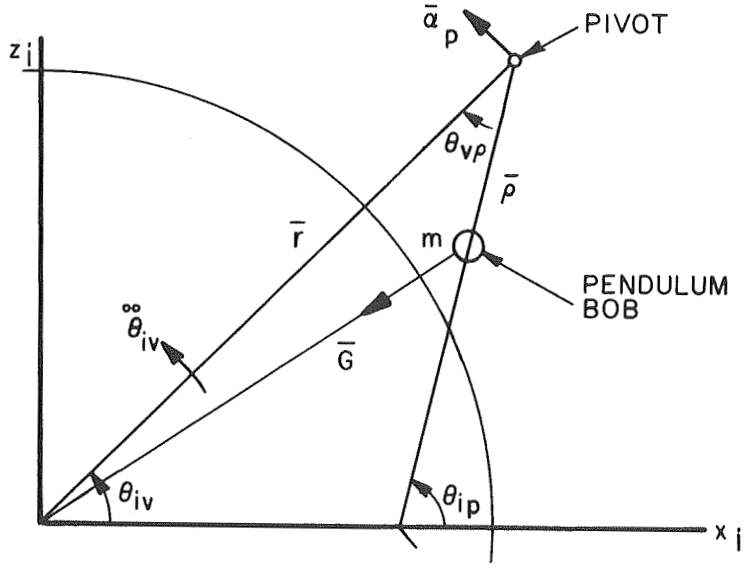

Figure 2.- Simple pendulum geometry

$$\bar{W}^{i}_{ip} = \begin{Bmatrix} 0 \\ -\dot{\theta}_{ip} \\ 0 \end{Bmatrix} \tag{9}$$

and where it is assumed that

$$[I] = \begin{bmatrix} I_{xx} & 0 & \\ & I_{yy} & \\ 0 & & I_{zz} \end{bmatrix}. \tag{10}$$

Substitution of Eqs. (3) through (10) into Eq. (2) yields the ideal equation of motion of the pendulum about its pivot which is given by

$$I_p \ddot{\theta}_{vp} + m\rho G\theta_{vp} = (m\rho R - I_p)\ \ddot{\theta}_{iv} \tag{11}$$

where

$$I_p = I_{yy} = m\rho^2 \tag{12}$$

Examination of Eq. (11) reveals that if the pendulum motion is to be insensitive to the acceleration of the pendulum pivot, then the coefficient of the acceleration term must be set to zero. Thus:

$$m\rho R = I_p. \tag{13}$$

This is the standard Schuler tuning condition and combination of Eqs. (12) and (13) reveals that in order to achieve Schuler tuning for a simple pendulum that

$$\rho = R. \tag{14}$$

This is, of course, impossible; therefore,consider a physical pendulum instead of a simple pendulum. In this case,

$$I_p = mk^2 \tag{15}$$

where k^2 is the radius of gyration.

Substitution of Eq. (15) into Eq. (13) reveals that the Schuler tuning requirement for a physical pendulum is given by

$$\rho = k^2/R \tag{16}$$

which, for reasonable values of k (i.e., k = 1 ft), results in a value of $\rho = 15 \times 10^{-7}$ cm which is of atomic dimensions. Thus it appears that construction of a Schuler-tuned pendulum is impossible.

In reference 1, Astrom and Hector suggest the application of an external torque about the pendulous axis in order to achieve a Schuler-tuned pendulum. This can be illustrated by rewriting Eq. (3) as

$$\bar{M}_p = \bar{\rho} \times \bar{F} + \bar{M}_{APP} \tag{17}$$

where

$$\bar{M}_{APP} = \begin{Bmatrix} 0 \\ M_p \\ 0 \end{Bmatrix}. \tag{18}$$

This results in a modification of Eq. (11) such that the motion of the pendulum about its pivot is given by

$$I_p \ddot{\theta}_{vp} + m\rho G\theta_{vp} = (m\rho R - I_p)\, \ddot{\theta}_{iv} + M_p \tag{19}$$

Next it is noted that if M_p is chosen as

$$M_p = -K_1 \ddot{\theta}_{ip}, \tag{20}$$

then Eq. (19) is further modified to

$$(I_p + K_1)\, \ddot{\theta}_{vp} + m\rho G\theta_{vp} = (m\rho R - I_p - K_1)\, \ddot{\theta}_{iv}. \tag{21}$$

Schuler tuning of this externally torqued pendulum is thus achieved by setting

$$K_1 = m\rho R - I_p. \tag{22}$$

Substitution of Eq. (22) into Eq. (21) results in the familiar pendulum equation:

$$\ddot{\theta}_{vp} + \omega_s^2 \theta_{vp} = 0 \tag{23}$$

where ω_s is the natural frequency of the system commonly called the Schuler frequency and is given by

$$\omega_s = \sqrt{G/R} \ . \tag{24}$$

The question of physical realizability, however, must still be resolved for this situation, since K_1 must indeed be large. Also, the problem of measuring $\ddot{\theta}_{iv}$ must be solved. This is discussed in Section III.

A signal flow diagram for the externally torqued, Schuler-tuned pendulum is presented in Figure 3, since it is the basic building block for the system signal flow diagrams to be presented in later chapters.

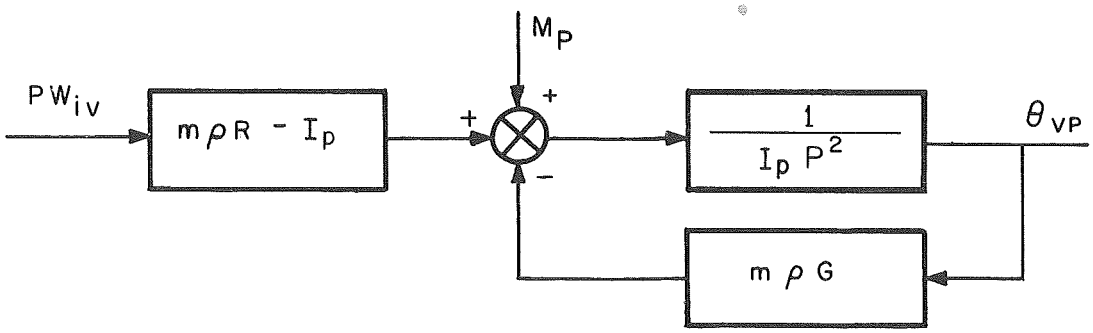

Figure 3.- Schuler-tuned pendulum

III. MEASUREMENT OF ANGULAR ACCELERATION WITH A SINGLE-DEGREE-OF-FREEDOM GYRO

The prime requirement for Schuler-tuning a pendulum according to the method proposed by Astrom and Hector (ref. 1) and described in the previous section is the ability to measure angular acceleration. One method would be to differentiate the output signal of a rate gyro. However, this is undesirable because of noise considerations and also because a more convenient technique (described below) is available.

The basic equation describing the performance of a single-degree-of-freedom gyroscope is derived in reference 6 and is given by

$$[I_g p^2+C_g p+K'_g]\ A_g = H_s [W_{IA}-W_{CMD}-A_g W_{SRA} + (u)W_g] - I_g p W_{oa}. \tag{25}$$

If the error terms $A_g W_{SRA}$ and $I_g p W_{oa}$ are neglected for the moment, a simplified block diagram of the gyro equation can be constructed as is illustrated in Figure 4.

Next, suppose that W_{CMD} is made proportional to the float angle A_g as well as to its integral such that

$$W_{CMD} = \frac{K_g + K_I/p}{H_s}\ A_g. \tag{26}$$

The signal flow diagram for this type of gyro is presented as Figure 5 and the gyro transfer function is given by

$$\frac{A_g}{p(W_{IA}+(u)W_g)} = \frac{H_s}{I_g p^3+C_g p^2+(K_g+K'_g)p + K_T}. \tag{27}$$

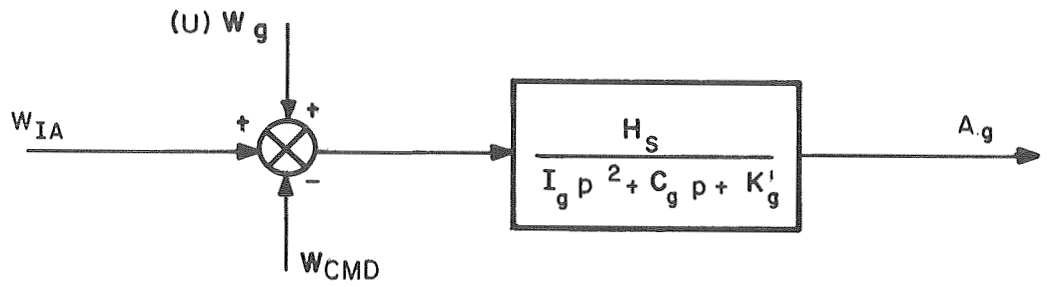

Figure 4.- Basic gyro signal flow

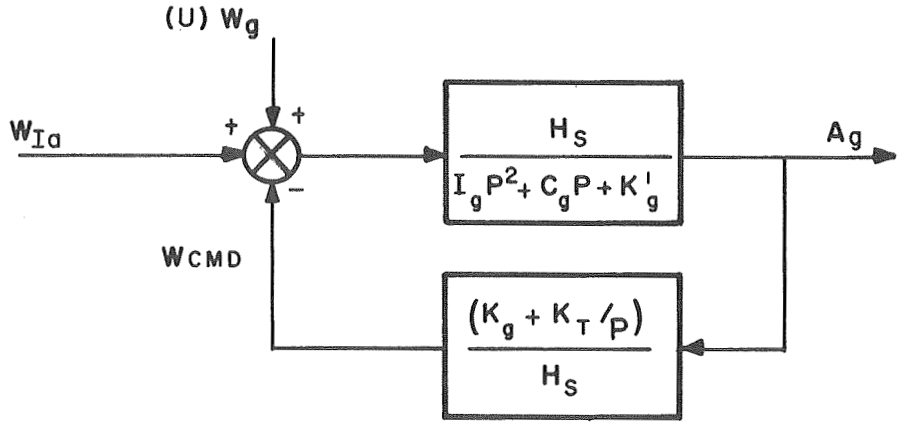

Figure 5.- Gyro signal flow with feedback

One should note from Eq. (27) that the use of proportional plus integral control in the feedback loop has made the gyro output angle A_g proportional to the input angular acceleration, and in steady state one obtains:

$$\left\{ \frac{A_g}{p(W_{IA}+(u)W_g)} \right\}_{ss} = \frac{H_s}{K_T} , \tag{28}$$

that is, the steady-state response to a step angular acceleration is a constant, as seen in Eq. (28), and to a step angular velocity is zero. Further, if one looks at the transfer function relating W_{IA} and W_{CMD}, one sees that

$$\frac{W_{CMD}}{W_{IA}+(u)W_g} = \frac{K_g p + K_T}{I_g p^3 + C_g p^2 + (K_g'+K_g)p + K_T} . \tag{29}$$

If $(u)W_g = 0$ and W_{IA} is a step, then the output angle A_g is zero and the steady-state value of W_{CMD} is given by

$$(W_{CMD})_{ss} = W_{IA} \tag{30}$$

which shows that in steady state the command angular velocity is equal to the input angular velocity.

Now, if the input angular velocity is $\dot{\theta}_{ip}$, then the command angular velocity is a measure of the velocity of the pendulum with respect to inertial space. Further, if the pendulum, is Schuler-tuned, then

$$\theta_{ip} \approx \theta_{iv} \tag{31}$$

and the command angular velocity of the gyro is a measure of the velocity of the vertical with respect to inertial space. Indication of the vertical could thus be obtained by integration of this signal.

It is apparent then that it is worthwhile to pursue this analysis further. To this end, consider the dynamic situation inferred by Eq. (29). One immediately notes a lag between input and output which should be kept small if the signal is to be used for vertical indication. Thus, the time constant of the lag term given by

$$\tau = K_g/K_T \tag{32}$$

should be kept much less than unity. Alternatively, this constraint can be written as

$$K_g/K_T << 1. \tag{33}$$

It should be possible to satisfy Eq. (33) since both K_g and K_T are arbitrary gains and are to be chosen to make the loop respond as desired. One desirable and mandatory feature of this loop is that it be stable. Application of the Routh Stability Criteria results in the requirement that

$$\frac{K_g' + K_g}{K_T} > \frac{I_g}{C_g}. \tag{34}$$

In the event that a single-axis integrating gyro is used to measure angular acceleration, Eq. (34) can be modified

$$K_g/K_T > \tau_g \tag{35}$$

since, for an integrating gyro, $K_g' = 0$ and

$$\tau_g = \frac{I_g}{C_g}. \tag{36}$$

Combining the requirements of Eqs. (33) and (35) results in bounding the ratio of the feedback gains, i.e.:

$$\tau_g < K_g/K_T << 1. \tag{37}$$

It is seen that Eq. (37) can be satisfied by choosing a single-degree-of-freedom gyro with a time constant of about 10^{-2} second which can be accomplished since, for heavily damped gyros, $\tau_g \sim 10^{-3}$ second and, for lightly damped gyros, $\tau_g \sim 10^{-1}$ second.

From a gyro design point of view, it is desirable that the float angle A_g be kept small as well as the angular velocity $\dot{A}_g$.

A frequency analysis of the transfer function relating A_g and W_{IA} shows that for the vehicle motions assumed in Section I the maximum float-angle displacement (assuming that the pendulum tracks the vertical perfectly) is on the order of 10 μrad, while the float angular velocity is on the order of 5×10^{-2} μrad/sec.

Thus, it appears that a single-degree-of-freedom gyro, with appropriate feedback torquing, can be used for measuring angular acceleration about the input axis.

This result, coupled with the requirement of Section II for Schuler-tuning a pendulum, leads to the mechanization of a Schuler-tuned pendulum or single-axis, vertical-indicating system as discussed in the next section.

IV. MECHANIZATION OF A SCHULER-TUNED PENDULUM

In Section II it was shown that a physical pendulum could be Schuler-tuned, provided that a torque which was proportional to the angular acceleration of the pendulum bob with respect to inertial space could be applied about the pendulum axis. In Section II it was shown that a single-degree-of-freedom gyro could be used to measure angular acceleration about its input axis by using proportional plus integral control in a feedback loop around the gyro (i.e., signal generator to torque generator). By combining these two concepts, it is possible to configure a single-axis Schuler-tuned pendulum as suggested by Astrom and Hector (ref.1). The mechanization of this type of pendulum is illustrated in Figure 6. A functional block diagram of the system is presented as Figure 7 and a signal flow diagram as Figure 8.

Note in Figure 8 the presence of a gyro-reaction torque $H_s(pA_g)$ which occurs because of the angular velocity of the float about the output axis.

The basic design problem associated with the indicated mechanization of the single-axis, Schuler-tuned pendulum is to choose the feedback gain $F(p)$ appropriately, such that the system is indeed Schuler-tuned. With reference to Figure 8 and with the uncertainties $(u)M_p^*$ and $(u)W_g$, disregarded, the following relations can be immediately written

$$M_p = [H_s p + F(p)]\, A_g \tag{38}$$

$$A_g = \frac{(H_s/C_g)}{p(\tau_g p+1)}\,(W_{ip}-W_{CMD}) \tag{39}$$

$$W_{ip} = W_{iv} + W_{vp} \tag{40}$$

$$W_{CMD} = (1/H_s)\,(K_g+K_T p)\,A_g \tag{41}$$

*Base motion coupling is assumed to be small and is treated as an uncertainty torque.

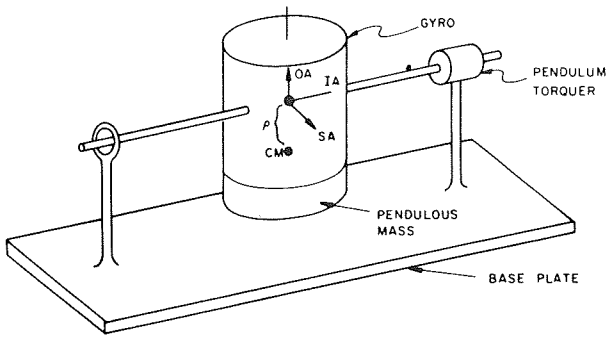

Figure 6.- Mechanization of a Schuler-tuned pendulum

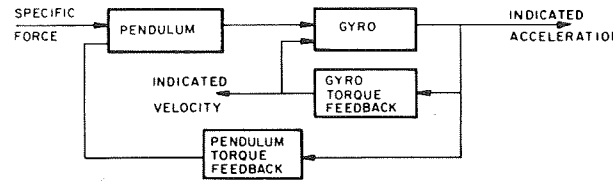

Figure 7.- Single-axis functional block diagram

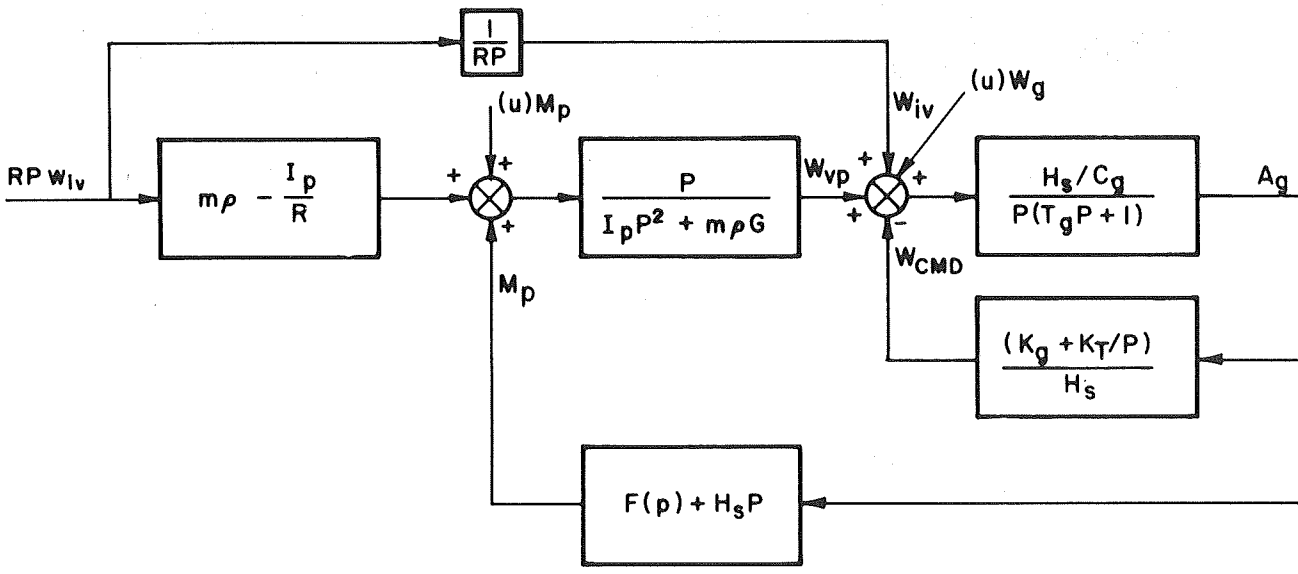

Figure 8.- Flow diagram of single-axis signal

$$W_{vp} = p[m\rho R - I_p)\ pW_{iv} + M_p]/[I_p p^2 + m\rho R] \tag{42}$$

$$\theta_{vp} = W_{vp}/p. \tag{43}$$

Combination of Eqs. (38) through (43) yields the transfer function relating (θ_{vp}), the angle between the pendulum and the vertical, and (pW_{iv}), the angular acceleration of the vertical relative to inertial space.

This results in

$$\left[\left(I_p p^2 + m\rho G\right)\left(\tau_g p^3 + p^2 + \frac{K_g}{C_g} p + \frac{K_T}{C_g}\right) - \frac{H_s}{C_g}\left(H_s p + F(p)\right) p^2\right] \theta_{vp}$$
$$= \left[\left(m\rho R - I_p\right)\left(\tau_g p^3 + p^2 \frac{K_g}{C_g} p + \frac{K_T}{C_g}\right) + \frac{H_s}{C_g}\left(H_s p + F(p)\right)\right] pW_{iv}. \tag{44}$$

Recall from Section II that Schuler-tuning was achieved by making the pendulum motion independent of the angular acceleration of the pivot. Applying the same concept to Eq. (44) results in the requirement that

$$F(p) = -\frac{C_g}{H_s}\left(m\rho R - I_p\right)\left(\tau_g p^3 + p^2 + \frac{K_g}{C_g} p + \frac{K_T}{C_g}\right) - H_s p \tag{45}$$

If Eq. (45) could be mechanized as the feedback gain, this would result in the motion of the pendulum with respect to the vertical being described by

$$m\rho R\left(p^2 + \frac{G}{R}\right)\left(\tau_g p^3 + p^2 + \frac{K_g}{C_g} p + \frac{K_T}{C_g}\right) \theta_{vp} = 0. \tag{46}$$

This is easily seen by the substitution of Eq. (45) into Eq. (44). Consider that the gyro gains K_g and K_T must be chosen as previously indicated for loop stability, such that the loop is fast compared to input and Schuler frequencies. If this is done, then Eq. (46) reduces, for low frequencies, to the familiar relation:

$$\left(p^2 + \frac{G}{R}\right) \theta_{vp} = 0. \tag{47}$$

Also, applying the same considerations to Eq. (45) and neglecting gyro reaction torque, one obtains the relation

$$F(p) \approx -\frac{K_T}{H_s}(m\rho R - I_p) \tag{48}$$

which also applies for low frequencies.

Before proceeding with the approximation to F(p) given by Eq. (48), it is instructive to proceed with the ideal feedback gain given by Eq. (45) to investigate the signals A_g, W_{CMD}, and M_p when the gyro and pendulum torquer uncertainties, $(u)W_g$ and $(u)M_p$, are non-zero. Again referring to Figure 8, and using Eq. (45), one can establish the following relations:

$$A_g = \frac{H_s p}{C_g G_2(p)} \left\{ W_{iv} + \frac{\left[(I_p p^2 + m\rho G)[(u)W_g] + p[(u)M_p]\right]}{m\rho R(p^2 + G/R)} \right\} \tag{49}$$

$$W_{CMD} = \frac{(K_g p + K_T)}{C_g G_2(p)} \left\{ W_{iv} + \frac{(I_p p^2 + m\rho G)[(u)W_g] + p[(u)M_p]}{m\rho R(p^2 + G/R)} \right\} \tag{50}$$

$$M_p = -(m\rho R - I_p)\, p \left\{ W_{iv} + \frac{(I_p p^2 + m\rho G)[(u)W_g] + p[(u)M_p]}{m\rho R(p^2 + G/R)} \right\} \tag{51}$$

$$G_2(p) = \tau_g p^3 + p^2 + \frac{K_g}{C_g} p + \frac{K_T}{C_g} \tag{52}$$

Examining Eqs. (49) through (52) for low-frequency response reveals that

$$G_2(p) \approx K_T/C_g \tag{53}$$

and

$$A_g \approx \frac{H_s}{K_T} p \left\{ W_{iv} + \frac{\frac{G}{R}\left[(u)W_g\right] + p\left[(u)M_p\right]/m\rho R}{(p^2+G/R)} \right\} \tag{54}$$

$$W_{CMD} \approx W_{iv} + \frac{\frac{G}{R}\left[(u)W_g\right] + p\left[(u)M_p\right]/m\rho R}{(p^2+G/R)} \tag{55}$$

$$M_p \approx -(m\rho R - I_p)p \left\{ W_{iv} + \frac{\frac{G}{R}\left[(u)W_g\right] + p\left[(u)M_p\right]/m\rho R}{(p^2+G/R)} \right\}. \tag{56}$$

Thus, all signals A_g, W_{CMD}, and M_p contain the required signal W_{iv} and are corrupted by gyro and pendulum torquer uncertainties in the same way. However, the most appropriate equation to use for obtaining the signal W_{iv} is W_{CMD}, since there is no integration or proportionality constant involved in the relation (55). However, it should be emphasized again that in the dynamic situation a lag between W_{CMD} and W_{iv} is involved, as was seen in Section III, and the gyro gains, K_g and K_T, must be chosen such that this lag is small.

This analysis is appropriate at low frequencies and, when perfect compensation (as given by Eq. (45)) is assumed, can be mechanized. In an actual situation, however, Eq. (45) cannot be mechanized and an imperfect compensator must be implemented and analyzed. The imperfect compensator which is immediately suggested is the low-frequency approximation of the perfect compensator given by Eq. (48). In this case, a constant gain which can be easily implemented is called for. As a second choice, one might consider a lead lag compensator such as

$$F(p) = -\frac{K_T}{H_s}(m\rho R - I_p)\left[\frac{\tau_1 p+1}{\tau_2 p+1}\right]. \tag{57}$$

By appropriate choice of τ_1 and τ_2, this compensator could be used to extend the bandwidth of the system beyond that which could be obtained by use of Eq. (48). Before choosing either of these forms, first consider the frequency characteristics of the perfect compensator in terms of typical sensor parameters and input motions.

Consider a single degree of freedom gyro with the following characteristics.

$H_s/C_g = 10$

$\tau_g = 10^{-2}$ sec

$m = 500$ gm

$\rho = 2$ cm

$I_p^* \doteq 8000$ gm-cm^2

$H = 2\times10^5$ gm-cm^2/sec

L = length = 10 cm

D = diameter = 6 cm.

By substitution of these values into Eq. (45), one obtains:

$$F(p) = -6.4\times10^{10}\,[10^{-2}p^3+p^2+0.5\times10^{-4}K_g p+0.5\times10^{-4}K_T] - \\ -2\times10^{+5}p \qquad (58)$$

It is desirable to choose the value of K_g such that the gyro-reaction torque can be neglected or, at most, treated as part of the uncertainty torque $(u)M_p$. To this end, choose

$$K_g \sim 2\times10^6 \text{ dyne-cm.} \qquad (59)$$

With this choice of K_g and recalling that for stability and small lag between W_{iv} and W_{CMD}

$$\tau_g < \frac{K_g}{K_T} << 1,$$

an appropriate choice of K_T appears to be

$$K_T \sim 1\times10^8 \text{ dyne-cm/sec.} \qquad (60)$$

---

*Note that I_p was calculated from the formulas for a right circular cylinder, i.e.:

$$I_p = m\left(D^2+\frac{L^2}{12}+\rho^2\right)$$

Substitution of Eqs. (59) and (60) into Eq. (58) appears to be

$$F(p) = - 6.4x10^{8} [p^3+100p^2+10,000p+500,000]$$

which can be rewritten as

$$F(p) = - 6.4x10^{8}(p+65)(p^2+35p+7725). \quad (61)$$

Thus, the first-order term has a break point at 65 rad/sec and the second-order term has a natural frequency of 88 rad/sec and a damping ratio of $\zeta = 0.2$. These frequencies are well above the Schuler frequency ($1.24x10^{-3}$ rad/sec) and the nominal velocity of the vertical relative to inertial space ($W_{iv} \sim 1.6x10^{-4}$ rad/sec). As a result of these calculations, it is appropriate to choose as the feedback gain

$$F(p) = - \frac{K_T}{H_s} (m\rho R - I_p),$$

which, on the basis of the above frequency analysis, should be accurate for frequencies up to about 10 Hz. Also note that gyro reaction torque can, in fact, be neglected on a numerical basis.

Based on the above conclusions, the signal flow diagram presented as Figure 9 applies and can be used to analyze the signals A_g, W_{CMD} and M_p.

From Figure 9 it is readily established that

$$\theta_{vp} = \frac{(m\rho R - I_p)}{G_1(p)} + \frac{M_p + (u)M_p}{G_1(p)} \quad (62)$$

$$M_p = \frac{K_T}{H_s} (m\rho R - I_p) A_g \quad (63)$$

$$A_g = \frac{(H_s/C_g)\ p\ (W_{ip} + (u)W_g)}{G_2(p)} \quad (64)$$

$$W_{ip} = W_{iv} + p\theta_{vp} \quad (65)$$

$$G_1(p) = I_p p^2 + m\rho G \quad (66)$$

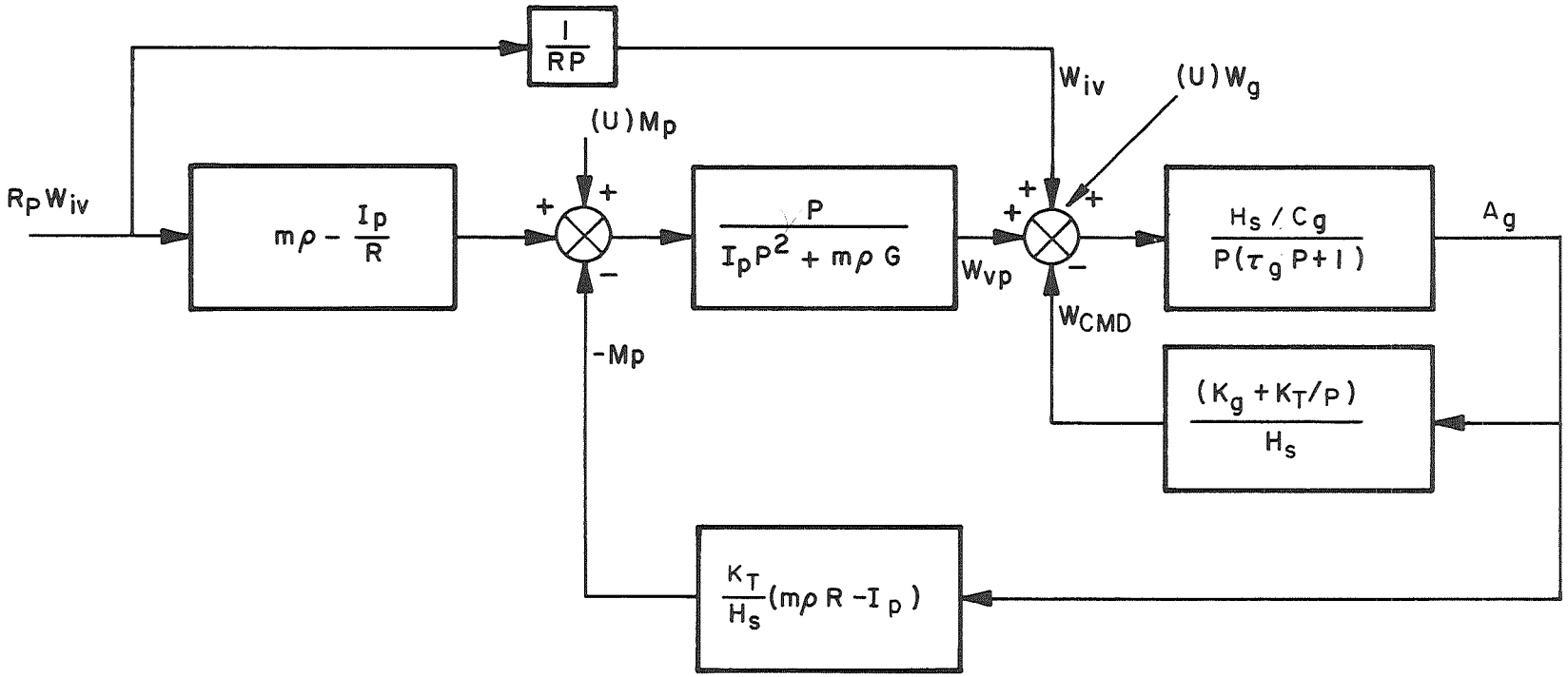

Figure 9.- Single-axis signal flow with gains specified

$$G_2(p) = \tau_g p^3 + p^2 + \frac{K_g}{C_g} p + \frac{K_T}{C_g} \tag{67}$$

Manipulation of Eqs. (62) through (67) results in the equation

$$[C_g G_2(p) G_1(p) + K_T p^2 (m\rho R - I_p)] A_g = H_s \left\{ G_1(p) p[(u) W_g] + \right.$$
$$\left. + p^2 [(u) M_p] + [G_1(p) + (m\rho R - I_p) p^2] p W_{iv} \right\}. \tag{68}$$

From Eq. (66), and the numerical values previously used, it is seen that the natural frequency of this undamped oscillator is approximately 12 rad/sec. However, it was previously shown that $G_2(p)$ has frequencies on the order of 65 to 88 rad/sec so that the product $G_1 G_2$ is well approximated by

$$G_1(p)\ G_2(p) \approx \frac{K_T}{C_g} G_1(p). \tag{69}$$

Substitution of Eq. (68) into Eq. (69) results in

$$A_g \approx \frac{H_s}{K_T} p \left\{ W_{iv} + \frac{(I_p p^2 + m\rho G)[(u) W_g] + p[(u) M_p]}{m\rho G (p^2 + G/R)} \right\}. \tag{70}$$

Similarly, it can be shown that

$$M_p \approx -(m\rho R - I_p) p \left\{ W_{iv} + \frac{(I_p p^2 + m\rho G)[(u) W_g] + p[(u) M_p]}{m\rho G (p^2 + G/R)} \right\}, \tag{71}$$

and that

$$W_{CMD} \approx \left(\frac{K_g}{K_T}\, p+1\right)\left\{ W_{iv} + \frac{(I_p p^2+m\rho G)\,[(u)W_g]+p[(u)M_p]}{m\rho R(p^2+G/R)} \right\}. \tag{72}$$

As previously shown, $\frac{K_g}{K_T} \approx 2\text{x}10^{-2}$ sec and $\sqrt{\frac{m\rho G}{I_p}}$ 12 rad/sec, while $\sqrt{G/R} \approx 1.24\text{x}10^{-3}$ rad/sec and $W_{iv} \approx 1.6\text{x}10^{-4}$ rad/sec. Thus, for frequencies of about 1 Hz the signals A_g, M_p, and W_{CMD} are well approximated by

$$W_{CMD} \approx W_{iv} + \left\{ \frac{\frac{G}{R}[(u)W_g]+p[(u)M_p]/m\rho R}{(p^2+G/R)} \right\} \tag{73}$$

$$A_g \approx \frac{H_s}{K_T}\, pW_{CMD} \tag{74}$$

$$M_p \approx -(m\rho R-I_p)\; pW_{CMD}, \tag{75}$$

which are identical with Eqs. (54), (55), and (56). For reasons cited previously it is appropriate then to use the W_{CMD} signal for navigation purposes. To this end, define

$$\dot{\theta}_{ivC} = W_{CMD} \tag{76}$$

$$\theta_{ivC} = W_{CMD}/p\,. \tag{77}$$

The errors $\delta\dot{\theta}$ and $\delta\theta$ and then defined by

$$\dot{\theta}_{ivC} = \dot{\theta}_{iv} + \delta\dot{\theta} \tag{78}$$

$$\theta_{ivC} = \theta_{iv} + \delta\theta. \tag{79}$$

Appropriate manipulation of Eqs. (73) and (76) through Eq. (79) results in

$$(p^2+G/R)\,\delta\dot{\theta} = \frac{G}{R}\,[(u)W_g] + \frac{p[(u)M_p]}{m\rho R} \tag{80}$$

$$(p^2+G/R)\;\delta\theta = \frac{G}{R}\,\frac{[(u)W_g]}{p} + \frac{[(u)M_p]}{m\rho R} \tag{81}$$

Finally, the offset angle between the pendulum and the vertical can be shown to be described by

$$(p^2+G/R)\;\theta_{vp} \approx \frac{(u)M_p}{m\rho R} - p[(u)W_g]. \tag{82}$$

This is accomplished by making the same approximations as were used to arrive at Eqs. (80) and (81).

In conclusion, it is seen that a constant feedback gain is appropriate for Schuler-tuning the single-axis system, and that with this gain the system will track motions up to about 1 Hz. It was also seen that gyro reaction torque could be neglected. It should also be noted that a perfect pendulum suspension was assumed in the above analyses and that any coupling of base motion into pendulum motion via imperfect suspension was small and would be treated as an uncertainty torque.

V. BASE MOTION ISOLATION OF A SCHULER-TUNED PENDULUM

In the previous section, coupling of the base angular motion with the pendulum motion was mentioned a number of times. This phenomenon could easily occur in the RAMP system if the pendulum suspension were not perfectly frictionless. In reality, the suspension is not frictionless, but can be built almost frictionless, particularly if the motion of the pendulum is kept small with respect to the base plate. This can be accomplished by employing a base-motion isolation system which would also cause the base plate to track the vertical approximately. Several additional advantages also accrue from base-motion isolation for the

single-axis case and most certainly when looking forward to a mechanization of a local vertical, North-pointing navigator. Among these advantages are:

1. The pendulum motion is kept small with respect to the base plate which simplifies construction of the suspension and aids in the pendulum torquer design (i.e., it is a null operating device).

2. Isolation from angular motion of the vehicle which helps prevent coupling of this motion into the pendulum is provided.

3. It allows for the mechanization of a North-pointing local vertical navigator.

To accomplish base-motion isolation in the single-axis case, a signal generator is mounted on the pendulus axis and a torque motor to drive the base plate is provided. Figure 10 illustrates how this system might be mechanized.

In this manner, the base plate is slaved to the local vertical without using the gyros, as is done in a conventional local vertical navigator. It is important to note in this mechanization that a nearly frictionless suspension of the gyro to the platform is required and that any friction in this suspension will contribute error to the system in the form of an interference torque. A signal flow diagram of this system is presented as Figure 11.

The subscripts CM refer to the controlled member which is defined to be the base-plate and pendulum assembly (see Figure 10). In this analysis, it is assumed that the base plate portion of the controlled member is designed such that the C.G. of the controlled member assembly is aligned with the pivot point of the base plate. Thus, no torques caused by vehicle acceleration will be exerted directly on the controlled member. The only torques which will be felt by the controlled member then will be those exerted on the pendulum pivot. These will be transferred to the controlled member pivot in the form of reaction torques. With these considerations, and from Figure 11, the equation describing the motion of the controlled member is written as

$$I_{CM}p^2\theta_{iCM} = m\rho RpW_{iv} - m\rho G\theta_{vp} + (M_p+(u)M_p) + (M_{CM}+(u)M_{CM}) \quad (83)$$

where $(u)M_{CM}$ includes effects of gyro-reaction torque, uncertainty in any applied torque M_{CM}, friction in the suspension, and the like. Also, note that

$$M_{CM} = F_{CM}(p)\ \theta_{CMp}. \quad (84)$$

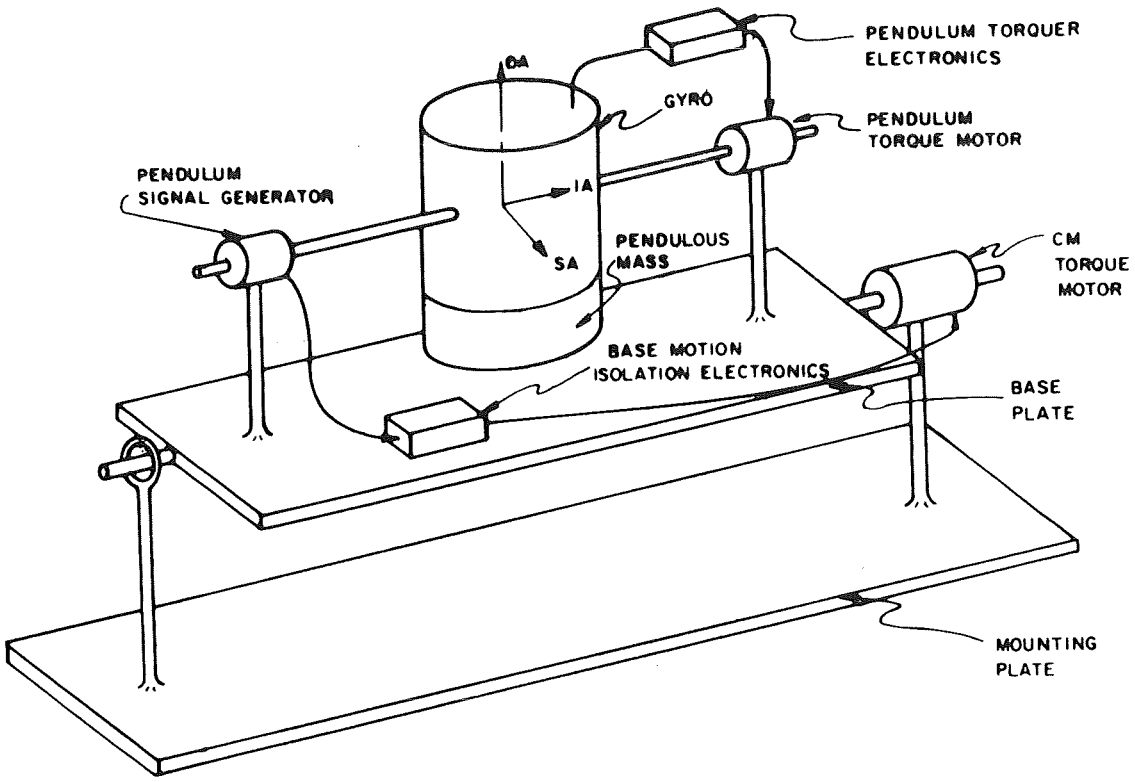

Figure 10.- Scheme of single-axis base-motion isolation

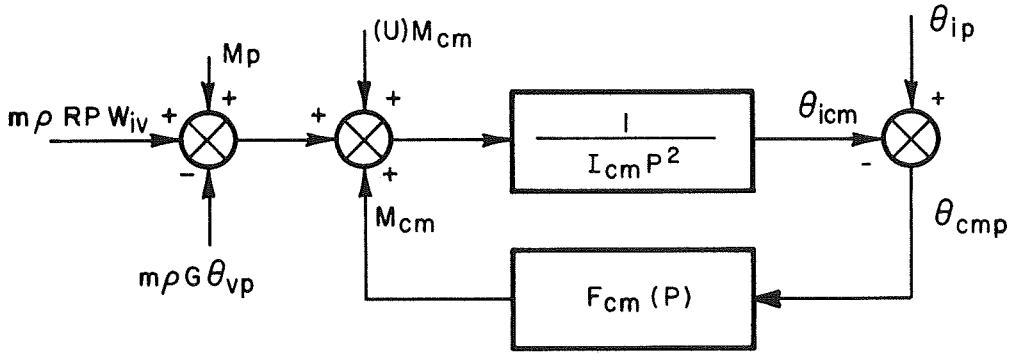

Figure 11.- Signal flow of single-axis, base-motion isolation system

The prime objective at this point is to design the feedback gain $F_{CM}(p)$ such that the angle θ_{CMp} between the pendulum and the controlled member is driven to zero resulting in the desired situation that

$$\theta_{iCM} = \theta_{ip}. \tag{85}$$

To design the gain $F_{CM}(p)$, begin by assuming that the uncertainties $(u)M_p$, $(u)M_{CM}$, $(u)W_g$, as well as the initial angle $\theta_{vp}(0)$, are zero.

This assumption results in

$$\theta_{vp} = 0 \tag{86}$$

$$\theta_{ip} = \theta_{iv}. \tag{87}$$

One also obtains the relation

$$M_p = -(m\rho R - I_p)\ pW_{iv}. \tag{88}$$

Let

$$F_{CM} = K \tag{89}$$

so that substitution of Eqs. (84) through (89) into Eq. (83) yields

$$I_{CM}p^2\theta_{iCM} = I_p p^2\theta_{iv} + K\theta_{CMv}. \tag{90}$$

But:

$$\theta_{iCM} + \theta_{CMv} = \theta_{iv}, \tag{91}$$

so that Eq. (90) can be rewritten as

$$\theta_{CMv} = \frac{(I_{CM}-I_p)\ pW_{iv}}{I_{CM}p^2 + K}. \tag{92}$$

From Eq. (92) it is obvious that it is impossible to drive θ_{CMv} identically to zero; however, it is possible to make θ_{CMv} fairly insensitive to input motions and to place its natural frequency high compared to Schuler frequency. This can be accomplished by choosing

$$K = I_{CM} W_{CM}^2 \tag{93}$$

where W_{CM} is large.

Substitution of Eq. (93) into Eq. (92) results in

$$(p^2+W_{CM}^2)\ \theta_{CMv} = \frac{(I_{CM}-I_p)}{I_{CM}}\ pW_{iv} \tag{94}$$

which, for an impulse pW_{iv}, yields an average value

$$\theta_{CMv} = 0, \tag{95}$$

and, for a step pW_{iv}, yields an average value

$$\theta_{CMv} = \frac{(I_{CM}-I_p)}{I_{CM}W_{CM}^2}\ . \tag{96}$$

This is certainly small since

$$\delta I = \frac{I_{CM} - I_p}{I_{CM}} << 1 \tag{97}$$

and I_{CM} is large.

The transfer function relating θ_{iCM} and θ_{iv} is easily derived by noting that

$$\theta_{iCM} + \theta_{CMv} = \theta_{iv}, \tag{98}$$

so that

$$\frac{\theta_{iCM}}{\theta_{iv}} = \frac{(p^2+\alpha^2 W_{CM}^2)}{(p^2+W_{CM}^2)} \tag{99}$$

where

$$\alpha^2 = I_{CM}/I_p > 1. \tag{100}$$

Equation (99) reveals that for low frequencies

$$\frac{\theta_{iCM}}{\theta_{iv}} \approx \alpha^2 \tag{101}$$

and, since α^2 is close to unity,

$$\theta_{iCM} \approx \theta_{iv} \tag{102}$$

for input frequencies close to the first break frequency W_{CM}. Note from these considerations the importance of the requirement that $I_{CM} \approx I_p$.

If the gain F_{CM} is found to produce undesirably high frequencies in the controlled member, then a lower frequency could be used but should be chosen well above the Schuler frequency, i.e., above

$$K \approx 10\ I_{CM}W_s^2. \tag{103}$$

It can also be shown that use of Eq. (93), including the effects of the uncertainties, results in

$$\theta_{iCM} \approx \theta_{iv} + \frac{1}{(p^2+G/R)}\left\{\frac{(u)M_p}{m\rho R} - p[(u)W_g]\right\} + \frac{(u)M_{CM}}{I_{CM}W_{CM}^2} \tag{104}$$

$$\theta_{CMv} \approx -\frac{1}{(p^2+G/R)}\left\{\frac{(u)M_p}{m\rho R} - p[(u)W_g]\right\} - \frac{(u)M_{CM}}{I_{CM}W_{CM}^2} \tag{105}$$

$$\theta_{CMp} \approx \frac{(u)M_{CM}}{I_{CM}W_{CM}^2} \tag{106}$$

which reveals that the dominant mode in the system is the Schuler mode. A signal flow diagram of the complete single-axis, vertical-indicating system, including a method for measuring the angle between the base and the vertical, is presented as Figure 12.

Before moving on to an error analysis of this system, one important consideration must be emphasized. In a conventional local vertical navigator, friction in the gimbal will cause base motion to be sensed directly by the gyro while in the RAMP system

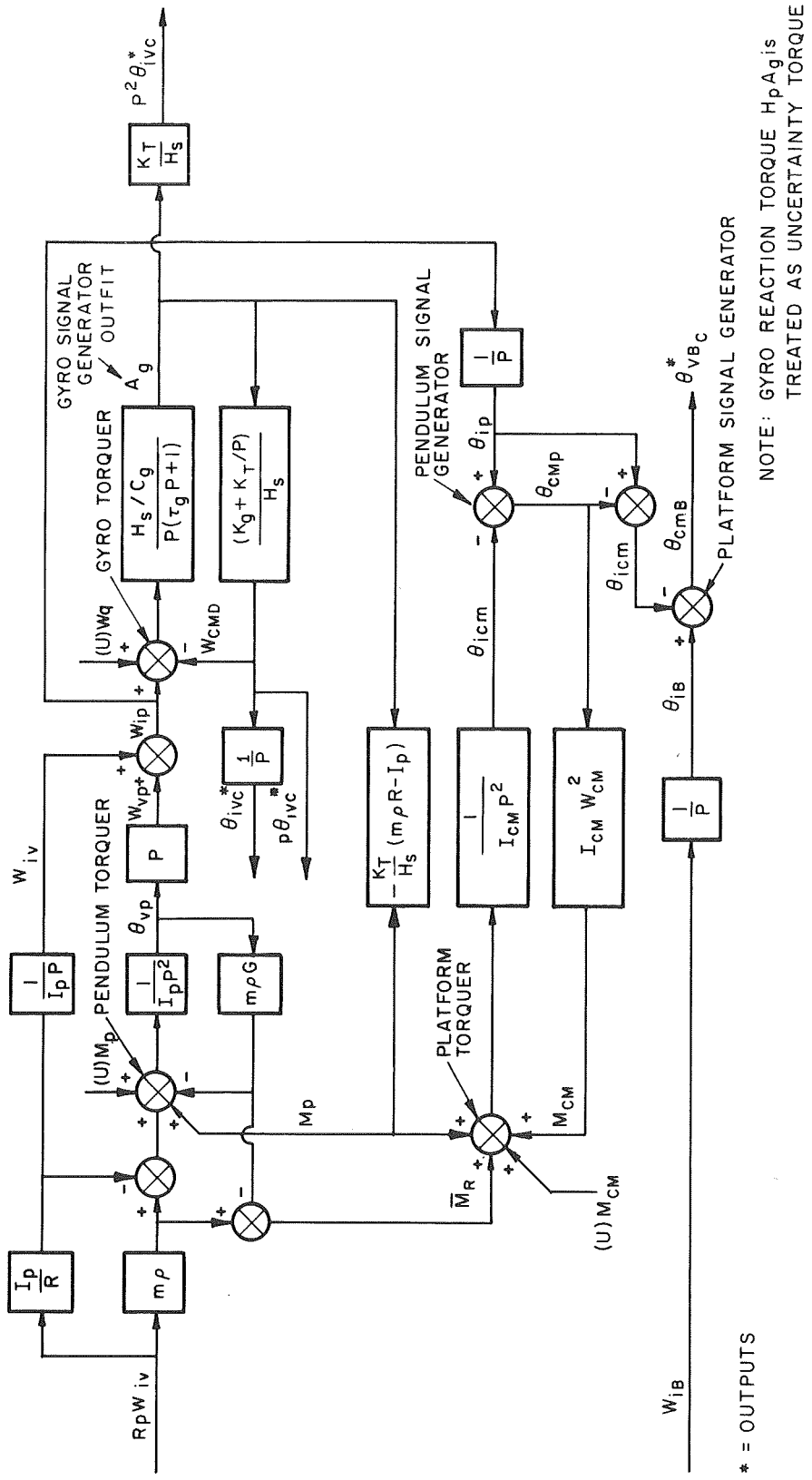

Figure 12.- Signal flow of single-axis, vertical-indicating system

friction in the gimbal will cause the platform not to track the vertical exactly, but coupling into the sensor will occur only if friction in the pendulum suspension also exists. This gives the RAMP system an advantage in that base motion coupling should be less than in a conventional system. This fact could result in a more stable operation of the gyros in the RAMP system than those in a conventional system.

VI. SINGLE-AXIS ERROR ANALYSIS AND EVALUATION

A major portion of the single-axis system error analysis has already been performed in the preceding sections of this work. For example, it has been shown, for frequencies of interest, that the errors in computer position and velocity are given by

$$\left(p^2 + \frac{G}{R}\right) \delta\dot{\theta} = \frac{G}{R}[(u)W_g] + p\,\frac{[(u)M_p]}{m\rho R} \tag{107}$$

and

$$\left(p^2 + \frac{G}{R}\right) \delta\theta = \frac{G}{R}\,\frac{[(u)W_g]}{P} + \frac{[(u)M_p]}{m\rho R}\,. \tag{108}$$

It has also been shown that the error angle between the pendulum and the vertical is given by

$$\left(p^2 + \frac{G}{R}\right) \theta_{vp} = -p[(u)W_g] + \frac{[(u)M_p]}{m\rho R} \tag{109}$$

and that the inability of the platform to track the vertical is described by

$$\left(p^2 + \frac{G}{R}\right) \theta_{CMv} = p[(u)W_g] - \frac{(u)M_p}{m\rho R} - \frac{(u)M_{CM}}{I_{CM}W_{CM}^2}\,. \tag{110}$$

Finally the error in slaving the platform to the pendulum was derived as

$$\theta_{CMp} = \frac{-(u)M_{CM}}{I_{CM}W_{CM}^2}\,. \tag{111}$$

In a conventional local vertical navigator (ref. 5), the errors in computed position and velocity are given by

$$\left(p^2 + \frac{G}{R}\right) \delta\dot{\theta} = \frac{G}{R}[(u)W_g] + \frac{p[(u)f]}{R} \tag{112}$$

$$\left(p^2 + \frac{G}{R}\right) \delta\theta = \frac{G}{R}\frac{[(u)W_g]}{p} + \frac{(u)f}{R} \tag{113}$$

where $(u)f$ is the uncertainty in measured specific force due to the accelerometer and $(u)W_g$ is the uncertainty in measured angular velocity due to the gyro.

By comparison of the RAMP error equations and the conventional local vertical navigator equations, one notes that gyro errors propagate identically in both systems. The comparison between accelerometer errors and pendulum torquer errors reveals that

$$\frac{(u)M_p}{m\rho} \Rightarrow (u)f. \tag{114}$$

Evaluation of the RAMP system is thus reduced to a comparison of accelerometer errors and torquer errors adjusted by appropriate proportionality constants. For purposes of this evaluation, therefore, consider that

$$|M_p|_{MAX} \sim |m\rho R p W_{iv}|_{MAX} \sim |m\rho f_{MAX}|. \tag{115}$$

With values for $r\ddot{I}_{MAX}$ from Section I and $m\rho$ from Section IV, it is easily established that

$$|M_p|_{MAX} = 500{,}000 \text{ dyne-cm.}$$

and

$$|f_{MAX}| = 0.5 \text{ g}$$

in horizontal directions.

It is also easily seen that

$$\left|\frac{(u)f}{f_{MAX}}\right| = \left|\frac{(u)M_p}{M_{pMAX}}\right| \tag{116}$$

so that, for equivalent performance, a 100-ppm accelerometer corresponds to a 100-ppm torquer. Thus, comparison of the two systems shows that identical error propagation will occur if identical gyros are used and if equivalent accelerometers and torquers are used. Of course, this assumes that these are the dominant error sources in the system which, to date, appears to be a valid assumption since, in general, gyro drift, accelerometer bias, and accelerometer scale factor are the dominant system errors in inertial navigators.

Currently, the state-of-the-art for accelerometers is on the order of 20 to 50 ppm. For a torque generator required to produce 500,000 dyne-cm, the state-of-the-art is on the order of 50 ppm which is comparable.

In a conventional local vertical navigator, the correction to the vertical (ref. 5) is given by

$$\left(p^2 + \frac{G}{R}\right) C_v = -p[(u)W_g] + \frac{(u)f}{R} . \tag{117}$$

By comparison of Eqs. (109) and (117) and by recalling Eq. (114), it is seen that

$$\theta_{vp} \Rightarrow C_v; \tag{118}$$

that is, the angle between the pendulum and the vertical in the RAMP system is equal to the correction to the vertical in a conventional system.

It will be recalled that the effect of the gyro reaction torque was included as part of the uncertainty torque $(u)M_p$. It is worthwhile at this point to evaluate the magnitude of this uncertainty and to compare it to the inherent physical torquer uncertainties. Denoting this uncertainty by $(u)T_G$, one can write that

$$(u)T_G = H_s p A_g \tag{119}$$

and, since

$$pA_g \approx \frac{H_s}{K_T} p^2 W_{iv}, \tag{120}$$

the numerical value for $(u)T_G$ is found to be

$$(u)T_G = \frac{H_s^2}{K_T} p^2 W_{iv} \sim 2.2\text{x}10^{-9} \text{ dyne-cm.} \qquad (121)$$

which is certainly negligible compared to inherent torquer uncertainties of 25 dyne-cm.

From the basic equations of error propagation given above, it has been established that equivalent errors in a conventional system will propagate identically in the RAMP system. This conclusion is valid whether the errors are deterministic or statistical in nature. On the assumption that the error sources $[(u)M_p]$ and $[(u)W_g]$ are statistically uncorrelated, have zero mean, and variances of σ_M^2 and σ_W^2, respectively, the errors in computed position velocity and attitude are given by

$$E(\delta\theta^2) = \left(t - \frac{\sin \omega_s t}{\omega_s}\right)^2 \sigma_W^2 + \frac{(1-\cos \omega_s t)^2}{(m\rho G)^2} \sigma_M^2 \qquad (122)$$

$$E(\delta\dot{\theta}^2) = (1-\cos \omega_s t)^2 \sigma_W^2 + \frac{\omega_s^2}{(m\rho G)^2} \sin^2 \omega_s t \, \sigma_M^2 \qquad (123)$$

$$E(\theta_{CMv}^2) = \frac{\sin^2 \omega_s t}{\omega_s^2} \sigma_W^2 + \frac{(1-\cos \omega_s t)^2}{(m\rho G)^2} \sigma_M^2 \qquad (124)$$

If the mean is non-zero, then it propagates in the deterministic manner dictated by Eqs. (107), (108), and (110).

VII. MECHANIZATION OF A LOCAL VERTICAL NAVIGATION SYSTEM

With allusion to the example of references 3 and 5, a local vertical navigation system will be mechanized which utilizes two RAMP's and one gyro. The RAMP's are used to sense the horizontal components of specific force and the gyro is used for azimuth control. Three gimbals will be employed to mechanize the base motion isolation system and a computer will be used for calculating compensation torques, position, and velocity. A functional block diagram for this system configuration is presented as Figure 13.

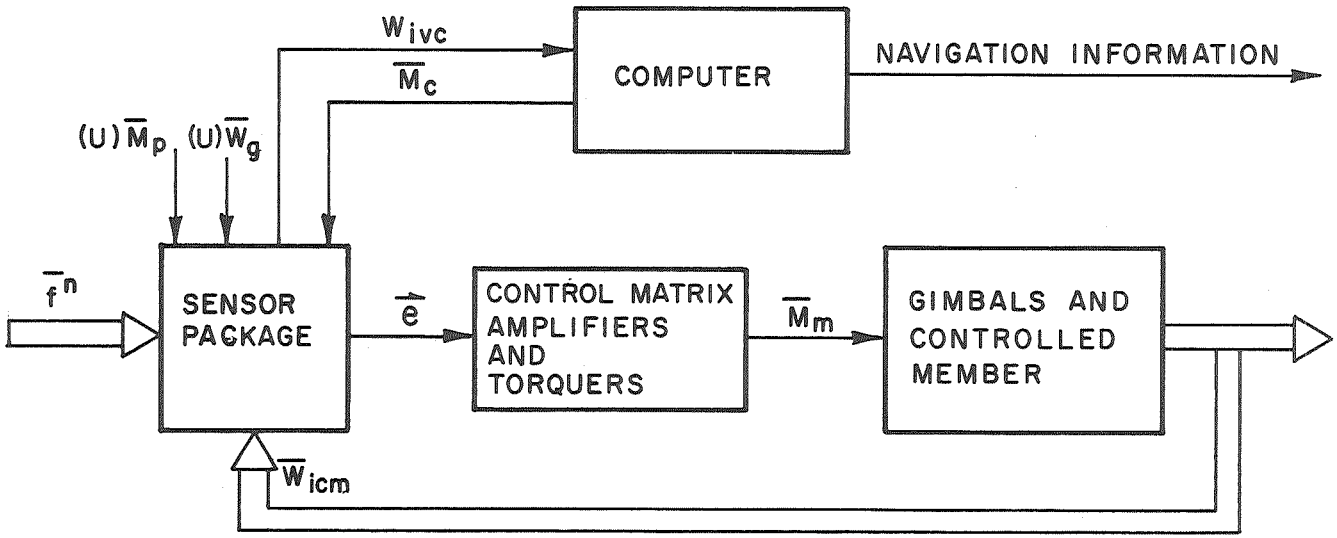

Figure 13.- Functional block diagram of RAMP vertical indicative system

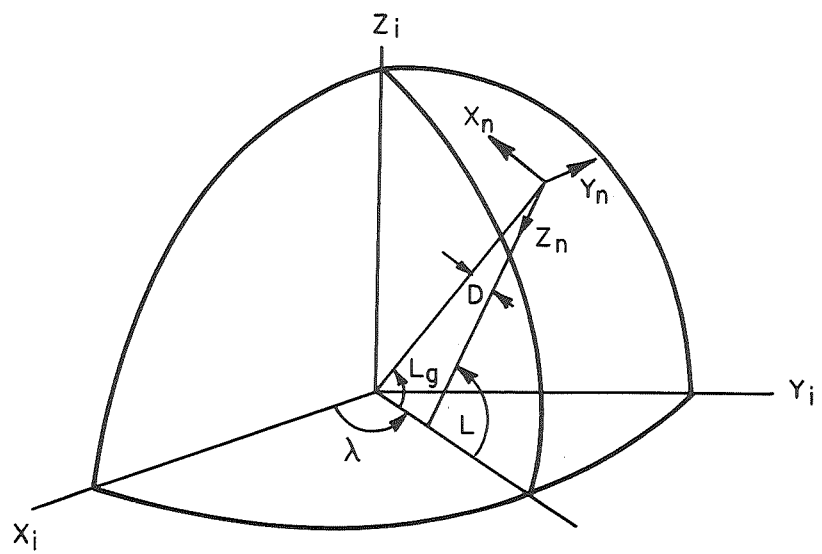

Figure 14.- Geometry of navigation coordinates

The system mechanization is based on the equations for specific force placed in coordinate form in the navigational frame illustrated in Figure 14. The equations for specific force in the navigational frame are given by

$$\bar{f}^n = C_i^n[\ddot{\bar{r}}^i - \bar{G}^i] \tag{125}$$

which, in component form for an elliptical, rotating Earth, are written as

$$\bar{f}^n = \left\{ \begin{array}{l} r_L\ddot{L} + \frac{1}{2} r_\ell(\dot{\lambda}^2 - \omega_{ie}^2) \sin 2L + 2\dot{r}_L\dot{L} - \ddot{r}\, e \sin 2L \\ \qquad -3e\, r \sin 2L\, \dot{L}^2 - \xi g \\ r_\ell\ddot{\lambda} \cos L - 2r_\ell\dot{L}\dot{\lambda} \sin L + 2\dot{r}_\ell\dot{\lambda} \cos L + \eta g \\ - g - \ddot{r} - r_L\ddot{L}\, e \sin 2L + r_\ell\, (\dot{\lambda}^2 - \omega_{ie}^2) \cos^2 L + \frac{r_L^2}{r}\dot{L}^2 \end{array} \right\} \tag{126}$$

where

$$r_L = r(1 - e \cos 2L) \tag{127}$$

$$r_\ell = r(1 + 2e \sin^2 L). \tag{128}$$

(See nomenclature for symbol definitions.)

Note that the effect of both the deviation of the normal and the deflection of the vertical is included in Eqs. (126), (127), and (128). Further, all terms of magnitude less than 20 μg have been neglected in accordance with the assumptions stated in Section I.

The angular velocity of the navigation frame with respect to inertial space is given by

$$\bar{W}_{in}^n = \left\{ \begin{array}{c} (\omega_{ie} + \dot{\ell}) \cos L \\ L \\ -(\omega_{ie} + \dot{\ell}) \sin L \end{array} \right\}. \tag{129}$$

A detailed mechanization of the system is given in Figure 15 and a simplified block diagram of the angular velocity sensor is presented as Figure 16. Examination of these figures illustrates the basic operation of the navigator, including the sensors, the position and velocity loops, the azimuth control loop, the compensation torques, and base-motion isolation.

The sensors and the position and velocity loops have been discussed in great detail in the preceding sections; however, it is necessary for the understanding of the system to describe in greater depth the nature of the compensation torques, azimuth control loop, and three-axis, base-motion isolation system.

The prime objective of this system is to indicate the vertical. To this end, it is necessary to compute latitude and longitude. Examination of Eq. (126) reveals that a number of terms, other than latitude and longitude, are present in the X_N and Y_N components of the specific force. These additional terms will then be calculated in the computer and appropriately subtracted from the system input by torquing the RAMP's with the negative of these values. By inspection then, the compensation torques can be written as

$$\begin{Bmatrix} M_{cx} \\ M_{cy} \end{Bmatrix} = \begin{bmatrix} C_x & 0 \\ 0 & C_y \end{bmatrix} \begin{Bmatrix} \frac{1}{2} r_\ell (\dot{\lambda}_i^2 - \omega_{ie}^2) \sin 2L_c + 2\dot{r}\dot{L}_c - \ddot{r}e \sin 2L_c \\ -2r_\ell \dot{L}_c \dot{\lambda}_c \sin L_c + 2\dot{r}_\ell \dot{\lambda}_c \cos L_c - 3er \sin 2L_c \dot{L}_c^2 \end{Bmatrix} \tag{130}$$

where

$$C_x = (m_x \rho_x - I_{px}/r_L) \tag{131}$$

$$C_y = (m_y \rho_y - I_{py}/r_\ell) \tag{132}$$

To calculate the compensation torques, it is noted that terms such as r, $\dot{r}$, and $\ddot{r}$ are required. To obtain these terms, an altimeter is used or, alternatively, a vertical accelerometer-altimeter combination could be used. A vertical accelerometer would also be useful in the system to aid in the calculation of gyro mass unbalance compensations. These types of compensations will not be discussed in this report, however, since they are identical to those which would be performed in a conventional system. The only point to be emphasized, however, is that a vertical accelerometer could possibly improve the accuracy of the RAMP navigator.

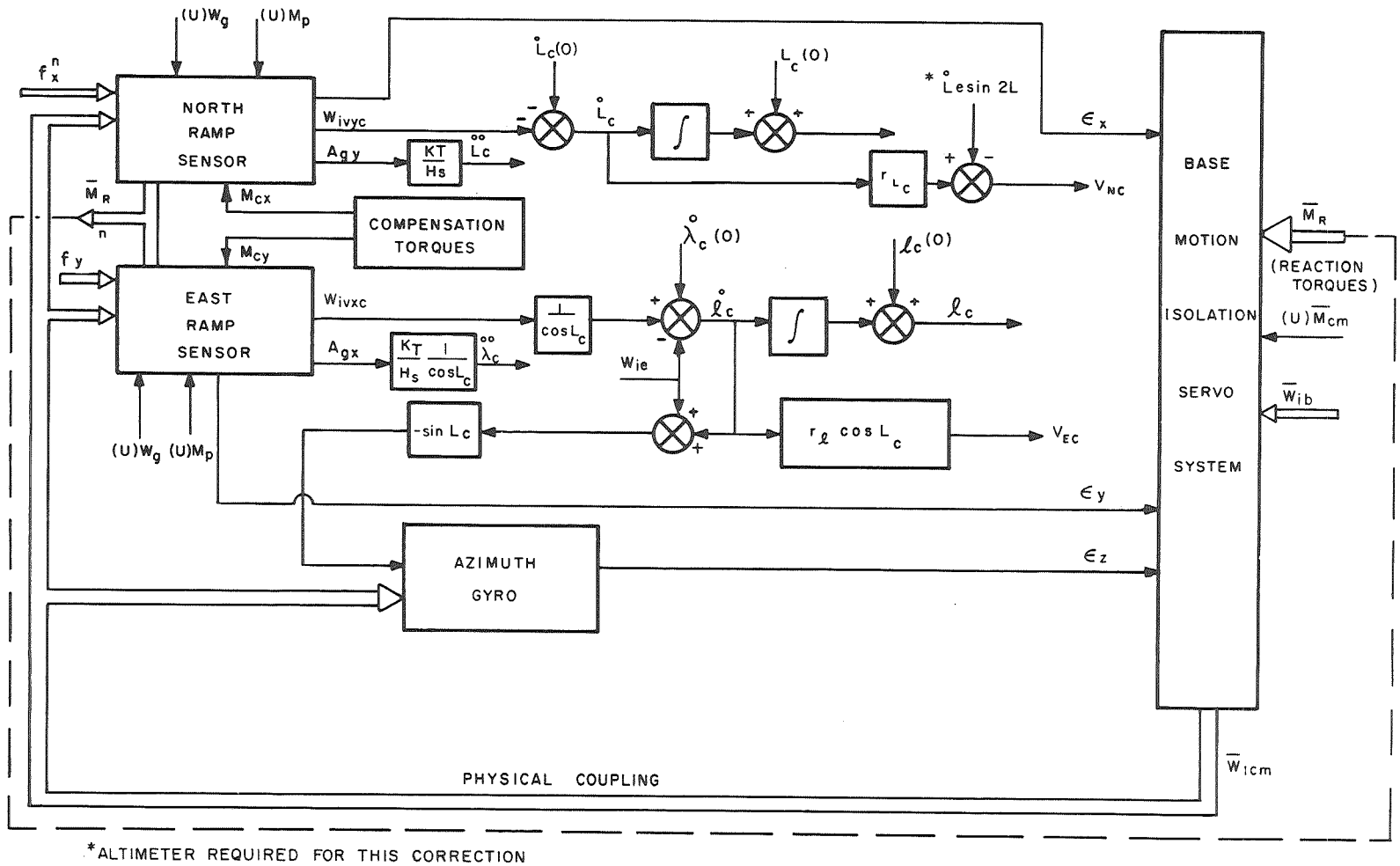

Figure 15.- Three-axis system mechanization

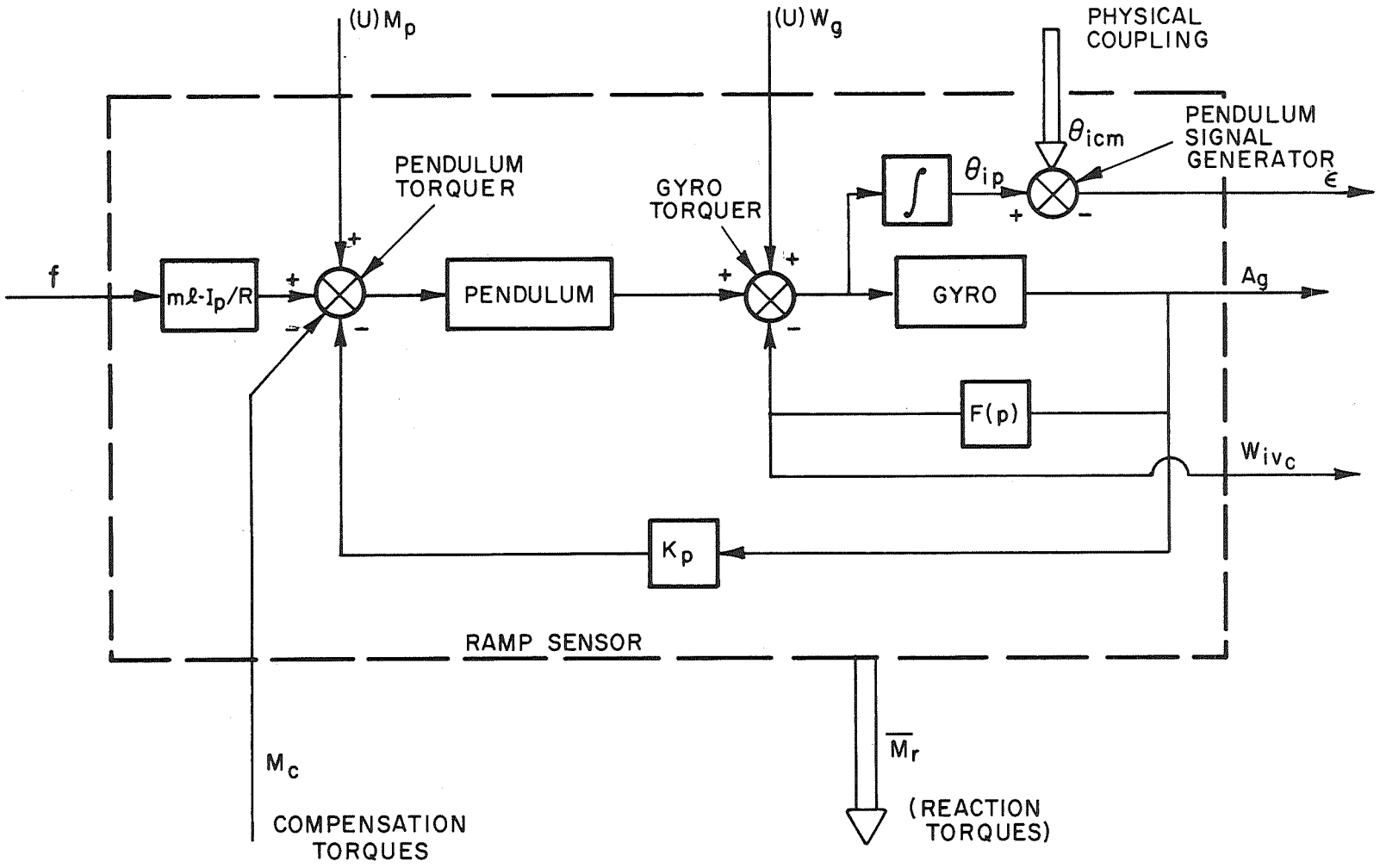

Figure 16.- Simplified block diagram of RAMP angular velocity sensor

If the compensations (130) are applied, then the outputs of the RAMP sensors are proportional to

$$\begin{Bmatrix} f_x \\ f_y \end{Bmatrix}^n = \begin{Bmatrix} r_L \ddot{L} - \xi g \\ r_\ell \ddot{\lambda} \cos L + \eta g \end{Bmatrix} + \begin{Bmatrix} \delta f_x \\ \delta f_y \end{Bmatrix} \tag{133}$$

where the δf terms are the result of using computed values in the torque compensation rather than the true values. This uncertainty will result in one of the types of uncertainty torques $(u)M_p$.

The azimuth control loop is identical to a conventional local vertical navigator azimuth loop and will, therefore, not be discussed separately, but rather as part of the base-motion isolation system. The basic configuration of the base-motion isolation (BMI) system is illustrated in Figure 17. The equations for governing the motion of the BMI system are rather complex and, since they are developed in detail in references 6 and 8, they will not be redeveloped in this report. However, the basic assumptions and resulting equations will be stated for the purpose of completeness.

The basic assumptions governing the developments in the above references are:

1. Each gimbal has a spherical ellipsoid of inertia.

2. Small changes of gyro angular momentum are negligible.

The error signals from the two RAMP's, as well as the signal from the azimuth gyro signal generator, are processed in the same manner as the commands to the gimbal servos in a conventional system. Figure 18 illustrates the method of processing these signals. The gimbal angles (Φ, θ, ψ) required for the signal resolution indicated in Figure 18 are obtained from signal generators mounted on the gimbal axes. The command to the gimbal torque motors is finally computed from

$$\overline{M}_{CM} = \begin{bmatrix} K_1 & 0 & \\ & K_2 & \\ 0 & & K_3 \end{bmatrix} \begin{Bmatrix} e_R \\ e_p \\ e_A \end{Bmatrix} \tag{134}$$

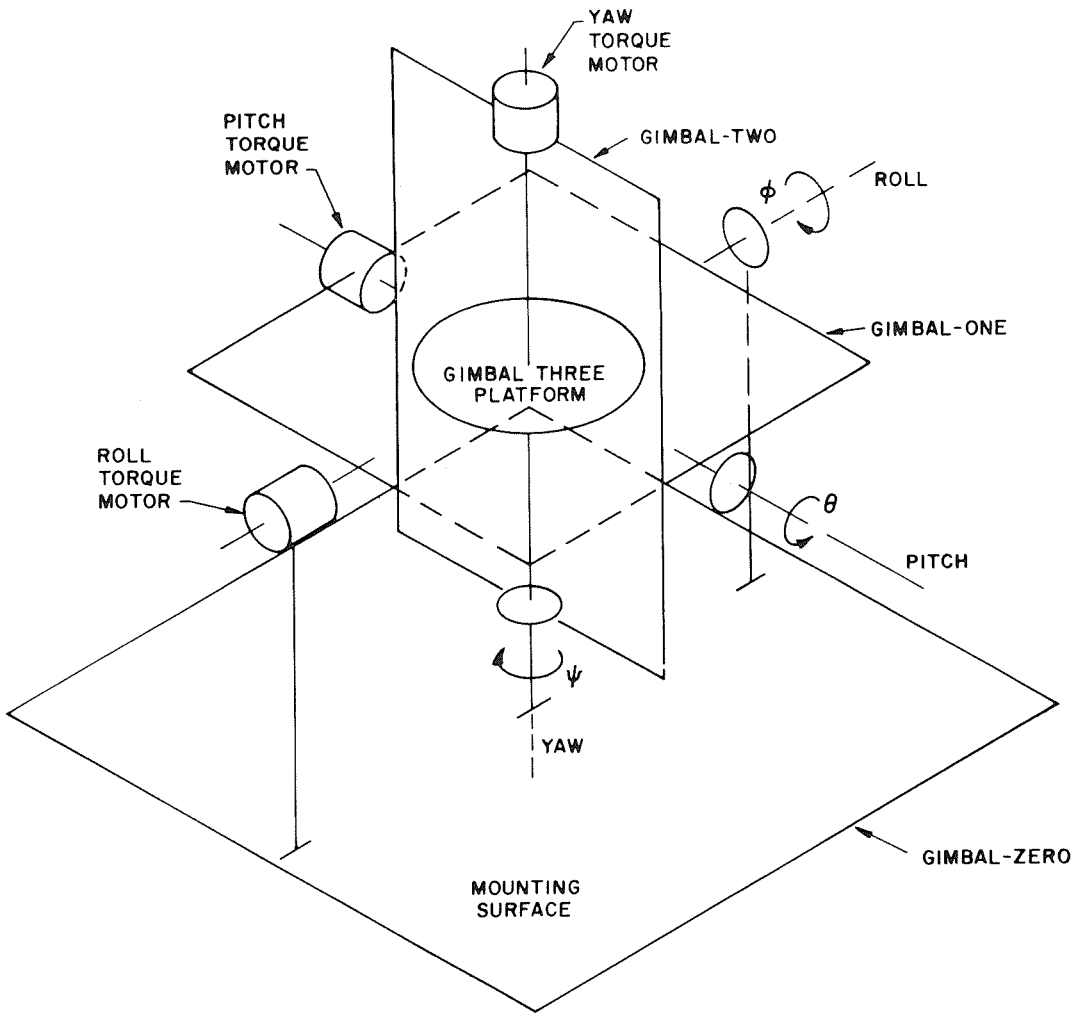

Figure 17.- Three-axis, base-motion isolation system

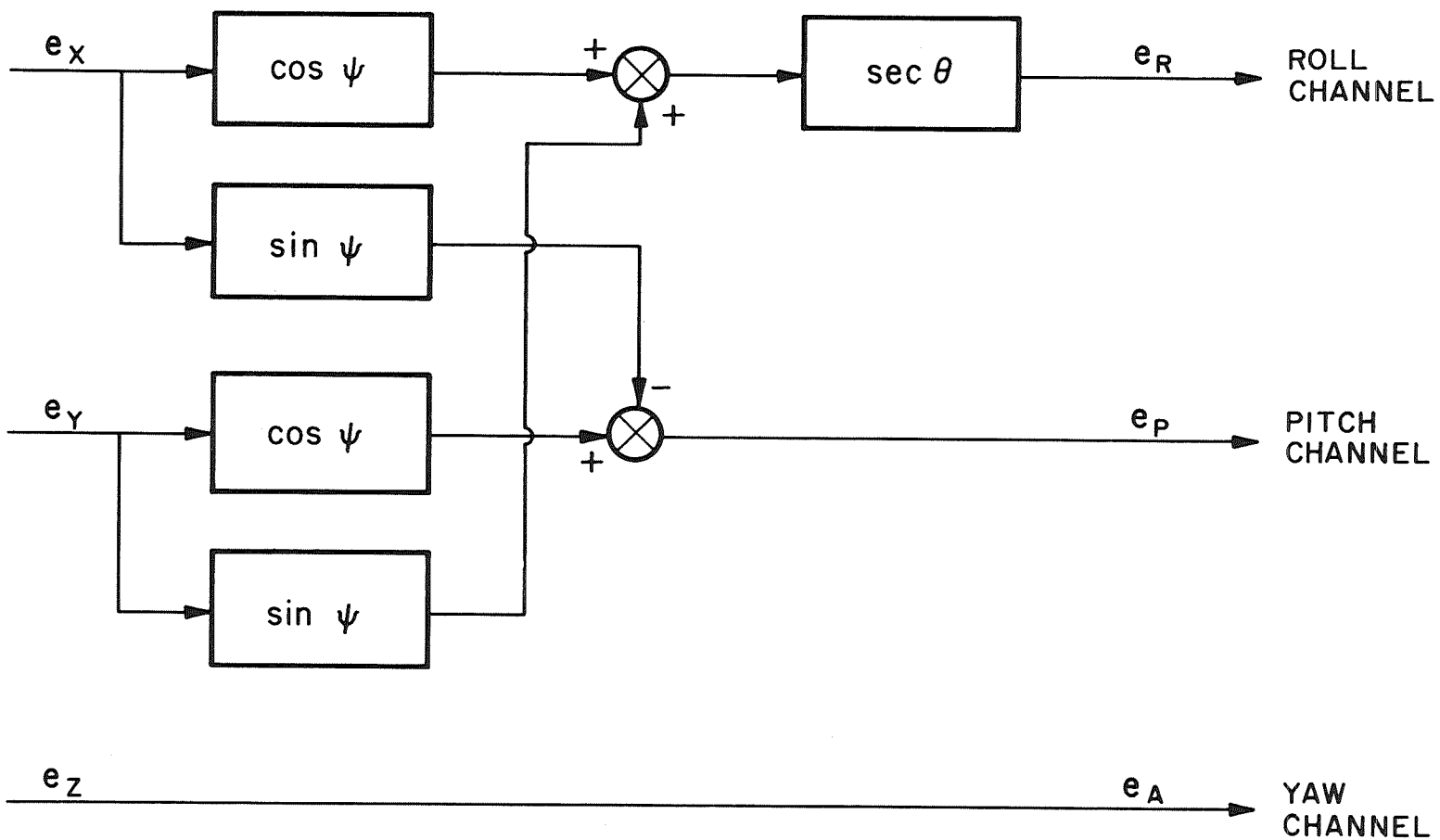

Figure 18.- Processing of BMI command signal

where the gains K_i are chosen according to the methods of Section IV (i.e., $K = I_{CM}W_{CM}^2$).

In Section IV, it was noted that the frequency W_{CM} should be high. This is also desirable in the three-axis case since cross-coupling caused by off-diagonal effects is minimized by making these gains large.

The one advantage of this mechanization over the conventional local vertical system is that a higher degree of base-motion isolation is achieved as was discussed in the single-axis case. It should also be noted that without the vertical gyro, navigation would be virtually impossible although, with a clock one could keep track of the vertical component of Earth rate and implement a free azimuth navigator in an open-loop fashion. However, this would be a very crude system to say the least.

VIII. ERROR ANALYSIS OF THE RAMP SYSTEM

For the single-axis RAMP system discussed in Section VI, it was found that error sources in the RAMP propagated in the same fashion as identical error sources in the conventional single-axis system. The error equations for the RAMP system will now be developed to determine whether this conclusion is valid in the three-axis case.

The dèrivation of the system error equations begins, as did the RAMP system mechanization, with the equations for specific force (see Eqs. (126), (127), and (128)). By defining a set of error angles (ε_N, ε_E, ε_z) resulting from positive rotations of the instrumented navigational frame about the true (positive) navigational axes, the actual components of specific force sensed by the instruments are given by

$$\bar{f}^p = [I-E^n]\,\bar{f}^n + \begin{bmatrix} 1/C_x & 0 \\ 0 & 1/C_y \end{bmatrix} (u)\bar{M}_p \qquad (135)$$

where the error matrix E^n is found from

$$C_p^n = \begin{bmatrix} 1 & \varepsilon_z & \varepsilon_E \\ \varepsilon_z & 1 & \varepsilon_E \\ -\varepsilon_E & \varepsilon_N & 1 \end{bmatrix} = I + E^n \quad . \qquad (136)$$

In the system mechanization (Figure 15), it has been assumed, however, that

$$\bar{f}^p = \bar{f}^n \tag{137}$$

and that

$$\begin{bmatrix} C_x & 0 & 0 \\ 0 & C_y & 0 \end{bmatrix} \bar{f}^p - \bar{M}_c = \begin{bmatrix} C_x & 0 \\ 0 & C_y \end{bmatrix} \begin{Bmatrix} \ddot{r_L} \\ r_\ell \ddot{\lambda} \cos L \end{Bmatrix} \tag{138}$$

where the quantities M_c, C_x, and C_y were previously defined by Eqs. (130), (131), and (132).

Thus, the system error equations are obtained from Eqs. (135), (137), and (138) and are written as

$$\begin{bmatrix} C_x & 0 & 0 \\ 0 & C_y & 0 \end{bmatrix} \bar{f}^n - \bar{M}_c - \begin{bmatrix} C_x & 0 & 0 \\ 0 & C_y & 0 \end{bmatrix} \begin{Bmatrix} E^n \bar{f}^n \end{Bmatrix} + (u)\bar{M}_p = \begin{bmatrix} C_x & 0 \\ 0 & C_y \end{bmatrix} \begin{Bmatrix} \ddot{r_L} \\ r_\ell \ddot{\lambda} \cos L \end{Bmatrix}. \tag{139}$$

Next, let

$$L_c = L + \delta L \tag{140}$$

$$\lambda_c = \lambda + \delta\lambda \tag{141}$$

and further assume that an altimeter is used to calculate r from the relation

$$r = r_o + h_a, \tag{142}$$

and that an altimeter error is defined by

$$\delta h = h_a - h. \tag{143}$$

Substitution of Eqs. (140) through (143) into Eqs. (126) and (130) yields, after extensive algebra, the equation:

$$\begin{bmatrix} C_x & 0 \\ 0 & C_y \end{bmatrix} \bar{f}^n - \bar{M}_c = \begin{bmatrix} C_x & 0 \\ 0 & C_y \end{bmatrix} \begin{Bmatrix} r_L \ddot{L} \\ r_\ell \ddot{\lambda} \cos L \end{Bmatrix} +$$

$$- \begin{bmatrix} C_x & 0 \\ 0 & C_y \end{bmatrix} \begin{Bmatrix} \xi g + r\delta\ddot{L} + 2\dot{L}\,\delta\dot{h} + r\dot{\lambda} \sin 2L\,\delta\dot{\lambda} + \ddot{L}\delta h \\ -\overline{\eta g} + \overline{r \cos L}\,\overline{\delta\ddot{\lambda}} + \overline{2[\dot{r} \cos L - r\dot{L} \sin L]}\,\overline{\delta\dot{\lambda}} + \\ - 2r\dot{\lambda} \sin L\,\delta\dot{L} - r[\ddot{\lambda} \sin L + 2\dot{L}\dot{\lambda} \cos L]\,\delta L + \\ + 2\dot{\lambda} \cos L\,\delta\dot{h} + \ddot{\lambda} \cos L\,\delta h \end{Bmatrix}. \tag{144}$$

It can also be shown that the term

$$\begin{bmatrix} C_x & 0 & 0 \\ 0 & C_y & 0 \end{bmatrix} \begin{Bmatrix} E^n \bar{f}^n \end{Bmatrix} = \begin{bmatrix} C_x & 0 \\ 0 & C_y \end{bmatrix} \begin{Bmatrix} -\varepsilon_z f_E + \varepsilon_E f_z \\ \varepsilon_z f_N - \varepsilon_N f_z \end{Bmatrix}. \tag{145}$$

This is accomplished by using Eq. (136) and by defining

$$\bar{f}^n = \begin{Bmatrix} f_N \\ f_E \\ f_z \end{Bmatrix}. \tag{146}$$

Substitution of Eqs. (144) and (146) into Eq. (139) finally results in the basic system error equations:

$$\xi g + r\delta\ddot{L} + 2\dot{L}\delta\dot{h} + r\dot{\lambda} \sin 2L\delta\dot{\lambda} + \ddot{L}\delta h - \varepsilon_z f_e + \varepsilon_E f_z + - (u) f_x = 0 \tag{147}$$

and

$$\eta g + r \cos L\delta\ddot{\lambda} + 2[\dot{r} \cos L - r\dot{L} \sin L]\,\delta\dot{\lambda} - 2r\dot{\lambda} \sin L\,\delta\dot{L} + -r[\ddot{\lambda} \sin L + 2\dot{L}\dot{\lambda} \cos L]\,\delta L + 2\dot{\lambda} \cos L\,\delta\dot{h} + \ddot{\lambda} \cos L\,\delta h + + \varepsilon_z f_N - \varepsilon_N f_z - (u)\, f_y = 0 \tag{148}$$

where

$$\begin{bmatrix} C_x & 0 \\ 0 & C_y \end{bmatrix} \begin{Bmatrix} (u)f_x \\ (u)f_y \end{Bmatrix} = (u)\bar{M}_p \tag{149}$$

Examination of Eqs. (147) and (148) reveals that these equations contain five unknowns. It remains then to find three additional equations in the five unknowns in order to describe the error propagation characteristics of the system completely.

The angular velocity of the instrumented frame with respect to inertial space is given by

$$\bar{W}^p_{ip} = C^p_n \bar{W}^n_{in} + \bar{W}^p_{np}. \tag{150}$$

Now consider the two torques to the RAMP's in addition to the torque applied to the vertical gyro. The torque applied to the vertical gyro is given by

$$-\dot{\lambda}_c \sin L_c \quad \text{(see Figure 15)},$$

so that the z component of the platform angular velocity with respect to inertial space in platform coordinates is given by

$$W_{ipz} = -\dot{\lambda}_c \sin L_c + (u)W_z \tag{151}$$

where $(u)W_z$ is the uncertainty in the z component of the angular velocity of the instrumented frame, which is caused by gyro drift, torquer scale factor, and so forth. Next, recall from the single-axis analysis that

$$W_{CMD} = W_{ivc} = W_{iv} + \frac{G}{R}\frac{[(u)W_g]}{(p^2+G/R)} + \frac{p[(u)M_p]}{m\rho R(p^2+G/R)} \tag{152}$$

and that

$$\theta_{vp} = \frac{[(u)M_p]}{m\rho R(p^2+G/R)} - \frac{p[(u)W_g]}{(p^2+G/R)} \tag{153}$$

Differentiation of Eq. (153) and substitution into Eq. (152) reveals that

$$W_{ivc} = W_{iv} + p\theta_{vp} + (u)W_g \tag{154}$$

$$W_{ivc} = W_{iv} + p\theta_{vp} + (u)W_g. \tag{155}$$

The relation is also easily established from Figure 9. From Eq. (154) it is obvious that

$$\bar{W}_{ip} = \bar{W}_{ivc} - (u)\bar{W}_g, \tag{156}$$

and from Eqs. (129), (151), and (156) that

$$\bar{W}^p_{ip} = \begin{Bmatrix} \dot{\lambda}_c \cos L_c - (u)W_{gN} \\ -\dot{L}_c - (u)W_{gE} \\ -\dot{\lambda}_c \sin L_c - (u)W_{gz} \end{Bmatrix}. \tag{157}$$

Again with use of Eqs. (140) and (141), it is easily shown that

$$\bar{W}^p_{ip} = [I+W^n]\ \bar{W}^n_{in} + (u)\bar{W} \tag{158}$$

where

$$(u)\bar{W} = -\begin{Bmatrix} (u)W_{gN} \\ (u)W_{gE} \\ (u)W_{gz} \end{Bmatrix} = \begin{Bmatrix} (u)W_N \\ (u)W_E \\ (u)W_z \end{Bmatrix} \tag{159}$$

(i.e., a negative gyro drift causes a positive angular velocity of the instrumented coordinate frame) and where

$$W^n = \begin{bmatrix} \delta\dot{\lambda}/\dot{\lambda} & 0 & \delta L \\ 0 & \delta\dot{L}/\dot{L} & 0 \\ -\delta L & 0 & \delta\dot{\lambda}/\dot{\lambda} \end{bmatrix}. \tag{160}$$

Equating Eqs. (158) and (150) and solving $\bar{W}^p_{np}$ yields

$$\bar{W}^p_{np} = [W^n + E^n]\ \bar{W}^n_{in} + (u)\bar{W}. \tag{161}$$

Noting that, in scalar form,

$$\bar{W}^n_{np} = \begin{Bmatrix} \varepsilon_N \\ \dot{\varepsilon}_E \\ \dot{\varepsilon}_z \end{Bmatrix} \tag{162}$$

one realizes that Eq. (161) represents the needed three-error equations. In scalar form, they are given by

$$\dot{\varepsilon}_N - \dot{L}\varepsilon_z + \dot{\lambda} \sin L\ \varepsilon_E = \cos L\ \delta\dot{\lambda} - \dot{\lambda} \sin L\ \delta L + (u)W_N \tag{163}$$

$$\dot{\varepsilon}_E - \dot{\lambda} \cos L\ \varepsilon_z - \dot{\lambda} \sin L\ \varepsilon_N = -\delta\dot{L} + (u)W_E \tag{164}$$

$$\dot{\varepsilon}_z + \dot{\lambda} \cos L\ \varepsilon_E + \dot{L}\varepsilon_N = -\dot{\lambda} \cos L\ \delta L - \sin L\ \delta\dot{\lambda} + (u)W_z. \tag{165}$$

Thus, five equations in the five unknowns have been obtained and can be written in the matrix form

$$A\bar{x} = \bar{G} \tag{166}$$

where

$$\bar{x} = \begin{Bmatrix} \varepsilon_N \\ \varepsilon_E \\ \varepsilon_z \\ \delta_L \\ \delta\lambda \end{Bmatrix} \tag{167}$$

$$\bar{G} = \begin{Bmatrix} (u)W_N \\ (u)W_E \\ (u)W_z \\ (u)f_N - \xi g - (\ddot{L}+2\dot{L}p)\ \delta h \\ (u)f_E + \eta g + \cos L\ (\ddot{\lambda}+2\dot{\lambda}p)\ \delta h \end{Bmatrix} \tag{168}$$

and where

$$[A] = \begin{bmatrix} p & \dot{\lambda}\sin L & -\dot{L} & \dot{\lambda}\sin L & (-\cos L)p \\ -\dot{\lambda}\sin L & p & -\dot{\lambda}\cos L & p & 0 \\ \dot{L} & \dot{\lambda}\cos L & p & \dot{\lambda}\cos L & (\sin L)p \\ 0 & (-g-\ddot{r}+r\dot{L}^2+ -r\dot{\lambda}^2\cos^2 L) & (2r\dot{L}\dot{\lambda}\sin L+ -r\ddot{\lambda}\cos L) & rp^2 & (r\dot{\lambda}\sin 2L)p \\ (g+\ddot{r}-r\dot{L}^2+ -r\dot{\lambda}^2\cos^2 L) & 0 & (r\ddot{L}+ +\frac{1}{2}r\dot{\lambda}^2\sin 2L) & -2r(\dot{\lambda}\sin Lp+ \dot{\lambda}\dot{L}\cos L+ +\frac{1}{2}\ddot{\lambda}\sin L & (r\cos L\ p+2\dot{r}\cos L- 2r\dot{L}\sin L)p \end{bmatrix} \tag{169}$$

At this point it is sufficient to notice that these equations are identical with those obtained for a conventional local vertical navigator (ref. 5).

Solutions are obtained by the methods of references 5 or 9 and will not be repeated here. Non-dimensional plots of error growth are also presented in these references.

The forcing function is also identical with the conventional navigator except that, as in the single-axis case, the accelerometer bias is replaced by the pendulum torquer uncertainty, i.e.:

$$\begin{bmatrix} m_x\rho_x & 0 \\ 0 & m_y\rho_y \end{bmatrix} \begin{Bmatrix} (u)f_x \\ (u)f_y \end{Bmatrix} = \begin{bmatrix} (u)M_{px} \\ (u)M_{py} \end{bmatrix} \tag{170}$$

Thus, it has been shown that the full RAMP navigation system has the same error-propagation mechanism as a conventional navigator, provided that the error sources are equivalent. If, however, the gyro drift rate is sensitive to float motion, the RAMP system

should be superior to a conventional system, since float motions of the gyro are smaller in the RAMP because of the base-motion isolation system and tight pendulum torquing loop than are the gyro float motions in a conventional system.

IX. CONCLUSIONS

Based upon the preceding analyses, it has been shown that the basic error propagation mechanism for a conventional local vertical navigator and the RAMP navigator are the same. Explanation of the high navigation accuracy with low accuracy components reported in reference 3 is therefore not explained in this way. At least two explanations of this phenomenon are possible. The first is that the gyro used in the RAMP system is susceptible to shifts in the drift compensation because of float motion and, since the RAMP base-motion isolation system and pendulum loop minimize this float by comparison to a conventional system, stable gyro drift terms which are compensable result. This effect is easily included in the error analysis, however, by appropriately including it in the forcing function terms $(u)\overline{W}$. An alternative explanation is that the gyros used are basically stable, once they are warmed up and calibrated, and that shifts would not occur except from warm-up to warm-up. In this event one system has no distinct advantage over the other from an accuracy standpoint. A definitive explanation is not possible, therefore, without extensive gyro testing to determine an appropriate model for $(u)\overline{W}$. The author has discussed the system with Mr. Folke Hector of the Swedish Philips Company, Ltd., of Stockholm, and he is essentially in agreement with the author's conclusions. One additional possible advantage of the RAMP system over a conventional system is cost, since no accelerometers are necessary in the RAMP system. Certain disadvantages or problems in construction of the RAMP system should also be noted. These are particularly apparent in the design of the pendulum suspension and the large pendulum torquer, as well as the requirement to align the pendulum axes with the gimbal axes.

Finally, mention should be made that the system could be fully digitized, mechanized as a free-azimuth navigator to eliminate azimuth tyro torquing uncertainty and, if inertial quality components are used, improved accuracies and warm-up to warm-up repeatability could be achieved.

REFERENCES

1. Astrom, K. J., and Hector, N. F.: Vertical Indication with a Physical Pendulum Based on Electromechanical Synthesis of a High Moment of Inertia. Report 590802 of the TTN-Group Division of Applied Hydromechanics, Royal Institute of Technology, Stockholm, Sweden, August 1959.

2. Astrom, K. J.: A Schuler-tuned Three Gyro Platform System. Report 591202 of the TTN-Group, Division of Applied Hydromechanics, Royal Institute of Technology, Stockholm, Sweden, December 1959.

3. Hector, F.: The RAMP Inertial Navigation System. Philips Technical Review, vol. 29, no. 3-4, 1968, pp. 69-85.

4. Markey, W., and Hovorka, J.: The Mechanics of Inertial Position and Heading Indication. Meuthen, London 1961.

5. Markey, W., and Britting, K. R.: Analysis of Local Vertical Inertial Navigation Systems. Experimental Astronomy Laboratory Report RE-52, Massachusetts Institute of Technology, March 1969.

6. Wrigley, W., Hollister, W. M., and Denhard, W. G.: Gyroscopic Theory Design and Instrumentation. Massachusetts Institute of Technology Press, Cambridge, Mass.

7. Halfman, R. L.: Dynamics: Particles, Rigid Bodies, and Systems, vol. 1, Addison-Wesley Publishing Co., Reading, Mass., 1962.

8. Schuler, M.: Phys. Zeit, vol. 24, 1923.

9. Broxmeyer, C.: Inertial Navigation Systems. McGraw-Hill Book Co., New York, 1964.

"The aeronautical and space activities of the United States shall be conducted so as to contribute . . . to the expansion of human knowledge of phenomena in the atmosphere and space. The Administration shall provide for the widest practicable and appropriate dissemination of information concerning its activities and the results thereof."

—NATIONAL AERONAUTICS AND SPACE ACT OF 1958

NASA SCIENTIFIC AND TECHNICAL PUBLICATIONS

TECHNICAL REPORTS: Scientific and technical information considered important, complete, and a lasting contribution to existing knowledge.

TECHNICAL NOTES: Information less broad in scope but nevertheless of importance as a contribution to existing knowledge.

TECHNICAL MEMORANDUMS: Information receiving limited distribution because of preliminary data, security classification, or other reasons.

CONTRACTOR REPORTS: Scientific and technical information generated under a NASA contract or grant and considered an important contribution to existing knowledge.

TECHNICAL TRANSLATIONS: Information published in a foreign language considered to merit NASA distribution in English.

SPECIAL PUBLICATIONS: Information derived from or of value to NASA activities. Publications include conference proceedings, monographs, data compilations, handbooks, sourcebooks, and special bibliographies.

TECHNOLOGY UTILIZATION PUBLICATIONS: Information on technology used by NASA that may be of particular interest in commercial and other non-aerospace applications. Publications include Tech Briefs, Technology Utilization Reports and Notes, and Technology Surveys.

Details on the availability of these publications may be obtained from:

SCIENTIFIC AND TECHNICAL INFORMATION DIVISION
NATIONAL AERONAUTICS AND SPACE ADMINISTRATION
Washington, D.C. 20546